Geological Society of America
Special Paper 409
2006

Magma-crust interactions and magma plumbing in a postcollisional setting: Geochemical evidence from the Erzurum-Kars volcanic plateau, eastern Turkey

Mehmet Keskin*
Istanbul University, Faculty of Engineering, Department of Geological Engineering, 34320 Avcilar, Istanbul, Turkey
Julian A. Pearce
School of Earth Sciences, Cardiff University, P.O. Box 914, Main Building, Park Place, Cardiff CF10 3YE, Wales, UK
Pamela D. Kempton**
Peter Greenwood
NERC Isotope Geosciences Laboratory, Kingsley Dunham Centre, Nicker Hill, Keyworth, Nottingham NG12 5GG, England, UK

ABSTRACT

In Northeastern Anatolia, the Erzurum-Kars plateau comprises the northernmost part of a volcanic province related to the collision between the Eurasian and Arabian continents. It contains an almost complete record of the volcanism from 11 Ma to 1.5 Ma. Volcanic units on the plateau are calc-alkaline in character and contain a distinct subduction signature. There was a systematic temporal variation in volcanic activity all over the plateau that can be seen in terms of three stages: it initiated with bimodal volcanic products between 11 and 6 Ma (the early stage), turned abruptly into a unimodal intermediate volcanism dominated by andesitic lavas between 6 and 5 Ma (the middle stage), and finally reverted to bimodal activity between 5 and 1.5 Ma (the late stage). These three stages were diachronous as the volcanic succession got progressively younger from the west to the east. The temporal variations were strongly dependent upon the depth of the magma chambers from which the volcanic products were derived. Lavas of the early and late stages were derived from relatively shallow chambers (<10–13 km) that fractionated anhydrous phases and assimilated a minor amount of crustal material or none. In contrast, those of the middle stage were sourced by large, deeper (>13 km), compositionally zoned chambers where amphibole was a fractionating phase and assimilation and fractional crystallization was an important process. The isotopic compositions of the volcanic units do not exhibit a systematic temporal variation on the Erzurum-Kars plateau; instead they exhibit spatial changes. Lavas from the western part of the plateau are much more unradiogenic in

*E-mail: keskin@istanbul.edu.tr.
**Present address: Natural Environment Research Council, Polaris House, North Star Avenue, Swindon SN2 1EU, UK.

Keskin, M., Pearce, J.A., Kempton, P.D., and Greenwood, P., 2006, Magma-crust interactions and magma plumbing in a postcollisional setting: Geochemical evidence from the Erzurum-Kars volcanic plateau, eastern Turkey, *in* Dilek, Y., and Pavlides, S., eds., Postcollisional tectonics and magmatism in the Mediterranean region and Asia: Geological Society of America Special Paper 409, p. 475–505, doi: 10.1130/2006.2409(23).

terms of their Pb isotopic ratios than those from the eastern part. These variations are possibly related to the composition and the amount of crustal material assimilated by the magmas, and hence indicate the existence of two different and isotopically distinct crustal domains beneath the plateau: (1) the Rhodope-Pontide fragment in the west and (2) the Northwest Iranian fragment in the east.

Keywords: eastern Anatolia; volcanism; continental collision; O, Sr, Nd, and Pb isotopes; magma plumbing; assimilation; assimilation and fractional crystallization; crustal domains

INTRODUCTION

Orogenic belts that formed by collisions between continents contain invaluable records of the geological history of the Earth, and therefore they have always attracted the attention of Earth scientists. The Eastern Anatolia region, exhibiting plateau morphology with an elevation of 1500–2000 m above sea level, is one of the two regions in the world in which an active continent-continent collision is currently taking place; the other is the Tibetan plateau (Şengör and Kidd, 1979; Dewey et al., 1986). Previous studies have shown that collision between the Eurasia and Arabia plates was responsible not only for the uplift of this extensive high plateau (Şengör and Kidd, 1979; Dewey et al., 1986), but also for the formation of a young and widespread volcanism, the products of which cover almost two-thirds of the region, masking older formations over great distances and reaching over 1 km in thickness in some places (Pearce et al., 1990; Keskin et al., 1998; Yılmaz et al., 1998). The Eastern Anatolia region is thus considered an ideal natural laboratory in which to study the early stages of a continent-continent collision and its effects.

Collision-related volcanic units of the Eastern Anatolian volcanic province span the whole compositional range, from basalts to rhyolites (Pearce et al., 1990; Notsu et al., 1995; Keskin et al., 1998). There is a gradual spatial change in the geochemical character of the volcanic units across the region in a north-south direction: volcanic units in the north around the Erzurum-Kars plateau, which represent the northernmost part of the province, are calc-alkaline in character with a distinct subduction signature, while those in the south are alkaline with a distinct within-plate signature (Pearce et al., 1990). The volcanic units in the north, around the plateau (Figs. 1 and 2), are of special interest not only because they contain a more complete record of volcanism from 11 Ma to 1.5 Ma, but also because the earliest volcanic activity in Eastern Anatolia initiated on this plateau (Keskin et al., 1998).

A detailed description and interpretation of the major- and trace-element geochemistry of around 300 whole-rock samples from the Erzurum-Kars plateau has been presented by Keskin et al. (1998). On the basis of major- and trace-element geochemistry, Pearce et al. (1990) and Keskin et al. (1998) have demonstrated that lavas of the plateau are calc-alkaline in character and display a broad compositional range, from basalts to rhyolites (Fig. 3). They have also demonstrated that all volcanic products contain a distinct subduction signature represented by the selective enrichment of large-ion lithophile elements and light rare earth elements relative to Nb, Ta, and other high field strength elements (Fig. 4). The Erzurum-Kars plateau has been divided into six subareas on the basis of volcanostratigraphy and geographic position (Keskin et al., 1998). From west to east, these are the (1) Mount Dumlu, (2) Mount Kargapazarı, (3) Pasinler, (4) Horasan, (5) Mount Aladağ, and (6) Kağızman subareas (Fig. 2). We retain this subdivision in this article in order to maintain the integrity of this article with our previous work.

The Keskin et al. (1998) study revealed that the collision-related volcanism on the Erzurum-Kars plateau had occurred in three consecutive stages: (1) early (11–6 Ma), (2) middle (6–5 Ma), and (3) late (5–2.7 Ma) (Fig. 2; see also Fig. 8 *in* Keskin et al., 1998). The aforementioned study also revealed that these three stages were diachronous, i.e., they began and ended in different parts of the plateau, the ages of the volcanic sequences becoming younger to the east. These three stages differed in many aspects: (1) the volcanic activity during the early and late stages was bimodal in character, while volcanism during the middle stage was unimodal (Fig. 3C); (2) the lavas and pyroclastic units of the early and late stages contain anhydrous crystallization assemblages dominated by plagioclase, pyroxenes, olivine, and oxides, whereas lavas of the middle stage are dominated by a hydrous (i.e., amphibole-bearing) fractionation assemblage (Keskin et al., 1998); and (3) the lavas of the middle stage display consistently higher degrees of crustal assimilation in comparison with those of the early and the late stages (Keskin et al., 1998). It should be noted that throughout this article we present the data both in terms of the six subareas and the three stages of volcanism in order to be able to reflect both spatial and temporal variations in magma chemistry across the Erzurum-Kars plateau.

In order to better understand the genesis of collision-related volcanism, the nature of the source regions, the evolution of the magma plumbing system, and the relative importance of various magmatic processes in magma chemistry across the Erzurum-Kars plateau, we conducted a Sr-Nd-O-Pb isotopic study on a subset of 23 representative lava samples, the major-oxide and trace-element data of which have already been published by Keskin et al. (1998). We selected these samples with special care in order to cover the whole stratigraphic sequence as well as the

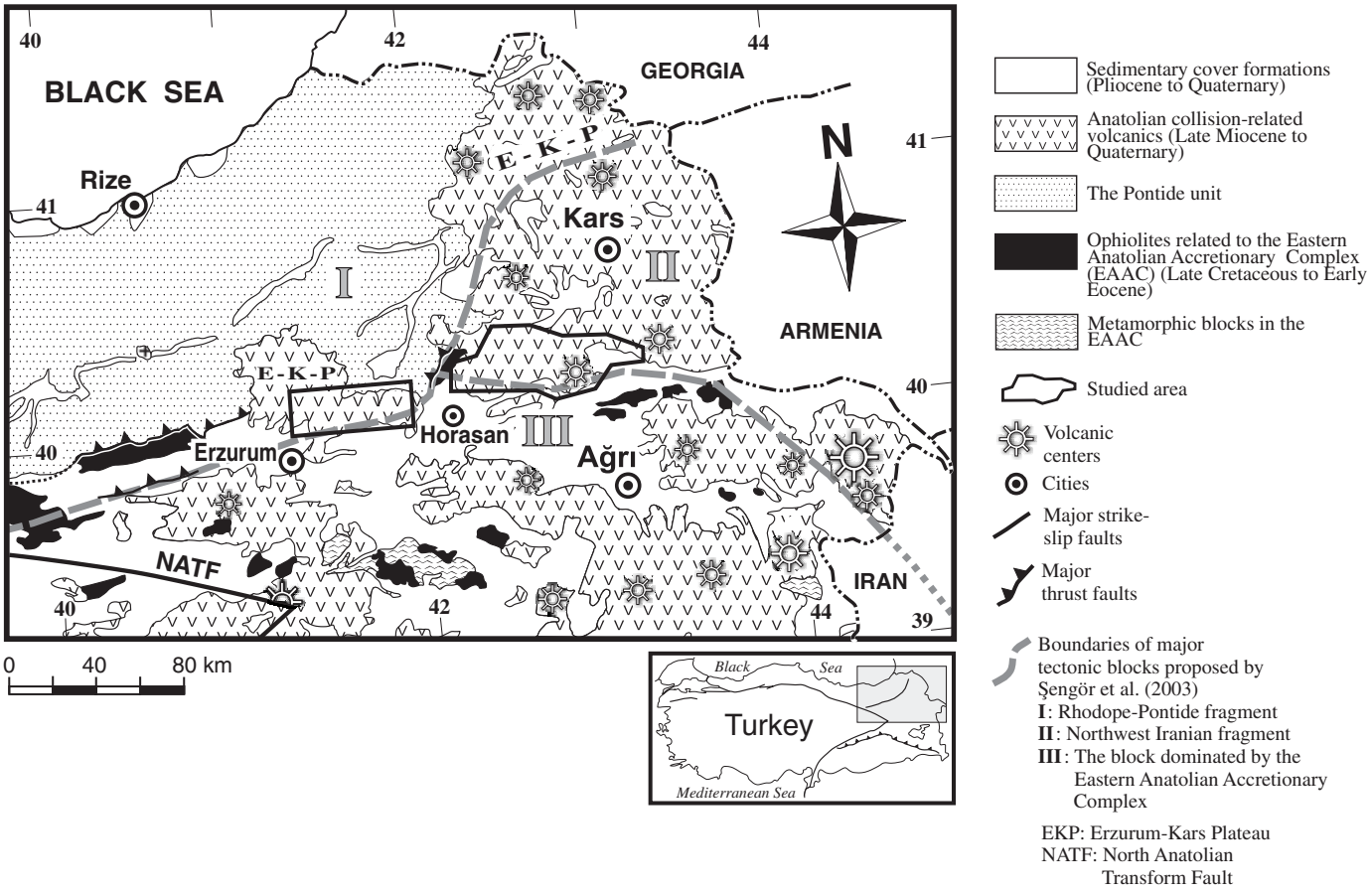

Figure 1. Location map displaying the study area, boundaries of major tectonic blocks (Şengör et al., 2003), and the distribution of collision-related volcanic units in northeastern Anatolia.

three stages of the volcanism (Fig. 2). Note that five of these samples (i.e., MK63, MK117, MK343, MK144, and MK175) had previously been radiometrically dated (Fig. 2 and Table 1). We also performed an electron microprobe study on phenocryst phases (e.g., plagioclases, pyroxenes, amphiboles) in a subset of hydrous lava samples from the Erzurum-Kars plateau. In this article, we report analyses only of amphiboles, because they have the potential of providing useful information about their depth of magmatic equilibration and hence the depth of magma chambers. We do not present microprobe analyses of other phases because of space limitations.

In this article, we specifically focus on the interpretation of magma-crust interactions and the evolution of the magma plumbing system beneath this part of the collision zone. Our aims for this article are (1) to introduce new Sr-Nd-Pb-O isotopic data from collision-related volcanic units of the Erzurum-Kars plateau, (2) to present spatial and temporal isotopic variations in these units, (3) to test whether these variations are related to source characteristics or governed by magma chamber processes, and finally (4) to propose a model for the evolution of the magma plumbing system beneath the plateau.

GEOLOGY

The basement of the Anatolian-Iranian plateau is made up of microcontinents that accreted to one another during the Late Cretaceous to the early Tertiary (Şengör, 1990). These microcontinents are separated by ophiolite belts and accretionary complexes. Three different tectonic blocks are known to exist in northeastern Anatolia: (1) the Rhodope-Pontide fragment in the north, (2) the Northwest Iranian fragment in the east, and (3) the Eastern Anatolian accretionary complex in the south (see the major tectonic blocks in Fig. 1). Collision-related volcanic products of the Erzurum-Kars plateau volcanic units (Pearce et al., 1990; Keskin et al., 1998) unconformably overlie these three tectonic blocks and so comprise the uppermost unit in the region. These units range in age from 11 Ma to recent and display great variability in their composition and eruptive character. The

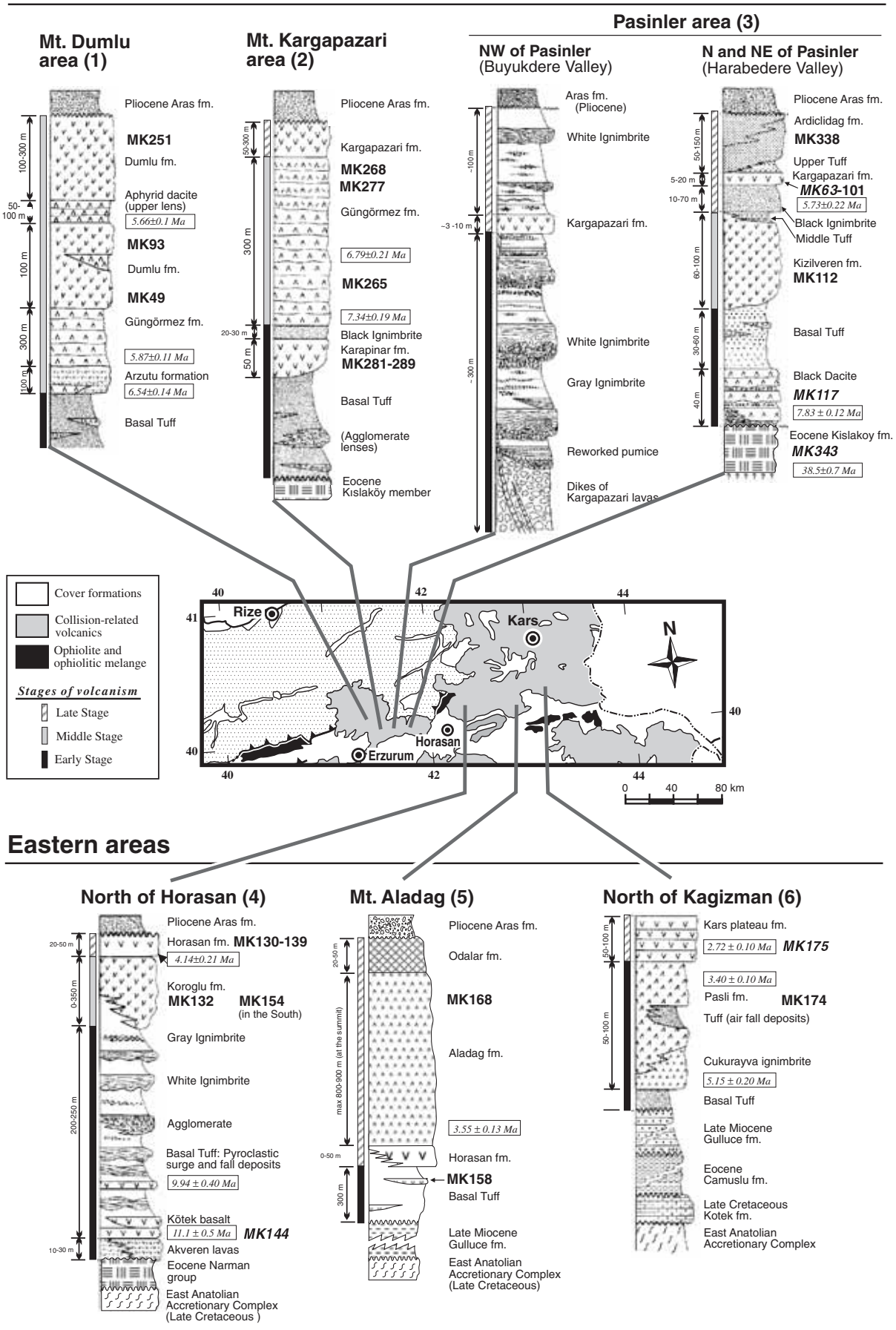

Figure 2. Location of the samples analyzed for Sr, Nd, Pb, and O isotopes on the Erzurum-Kars plateau. The samples are presented on generalized volcanostratigraphic sections of the six subareas on the plateau. Italics are used for the samples dated by the K/Ar method, and the numbers in frames are eruption ages in millions of years (Keskin et al., 1998).

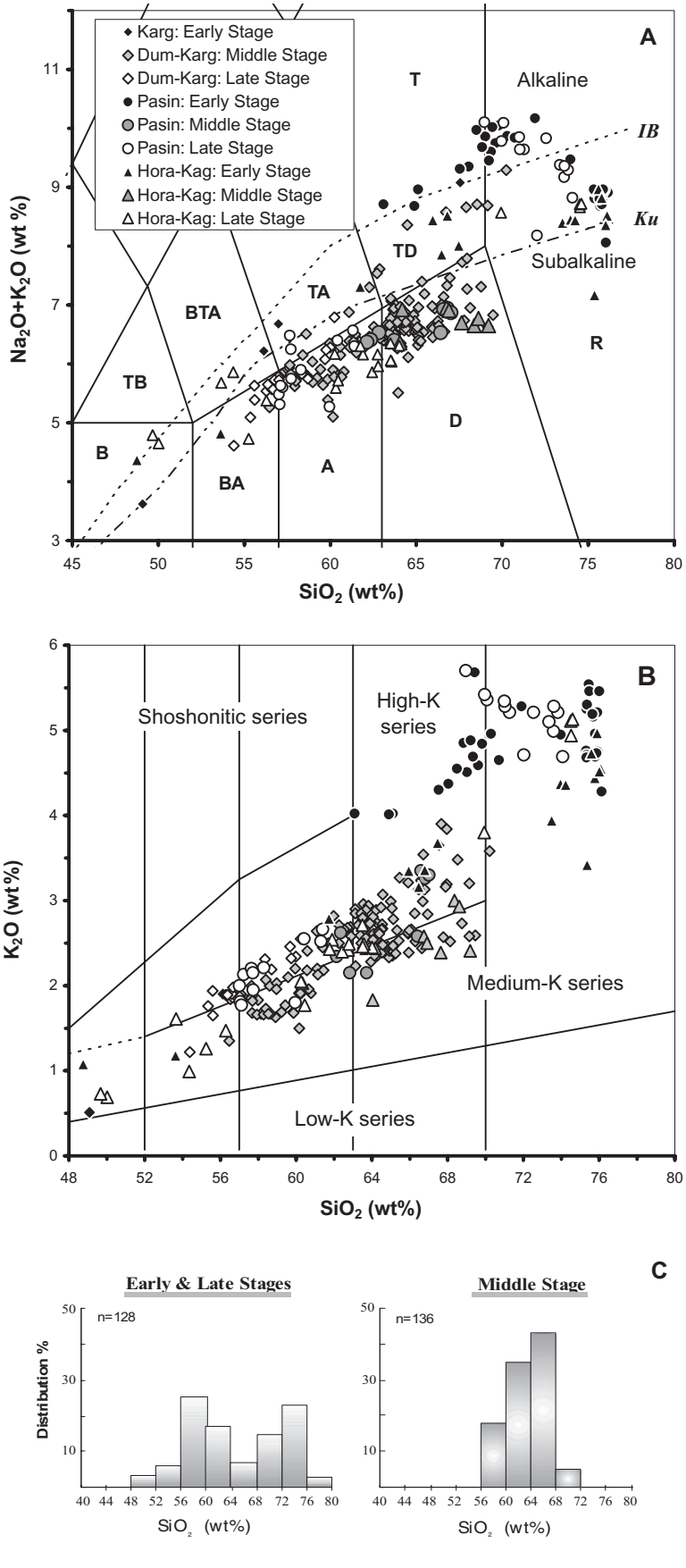

Figure 3. Classification of Erzurum-Kars plateau volcanic rocks utilizing (A) the total alkali versus SiO_2 (TAS) diagram of Le Bas et al. (1986) and (B) the K_2O versus SiO_2 diagram of Peccerillo and Taylor (1976). (C) Histograms of SiO_2 values showing the distribution of silica in the lavas of the middle and early/late stages. Major-element data are from Keskin et al. (1998). A—andesite; B—basalt; BA—basaltic andesite; BTA—basaltic-trachyandesite; D—dacite; R—rhyolite; T—trachyte; TA—trachyandesite; TB—trachybasalt; TD—trachydacite. The line marked as Ku in (A) divides the subalkaline field (the area located below) from the alkaline field (Kuno, 1966). IB—alkaline-subalkaline divide of Irvine and Baragar (1971). The abbreviations in the legend indicate subareas on the plateau: Karg—Mount Kargapazarı; Dum—Mount Dumlu; Pasin—Pasinler; Hora—Horasan; Kag—Kağızman.

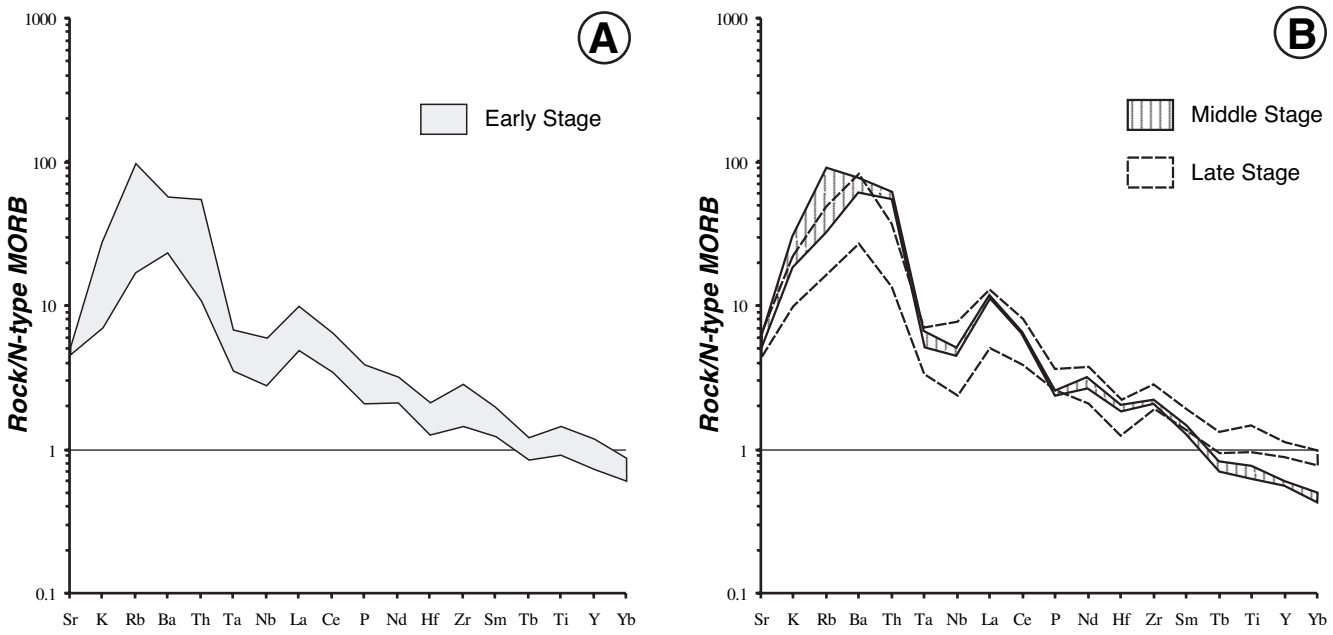

Figure 4. Comparison of N-type MORB-normalized trace-element patterns for representative samples from the (A) early stage and (B) the middle and late stages of the volcanism across the Erzurum-Kars plateau. The patterns for each stage of the volcanic activity on the plateau have been taken from the data presented in Keskin et al. (1998). The normalization values are from Sun and McDonough (1989). The elements are arranged in the order proposed by Pearce (1983).

volcanostratigraphy and eruptive character of the units of the plateau are thoroughly discussed in previous work (Keskin et al., 1998) and hence are not reiterated here.

The western part of the Erzurum-Kars plateau (i.e., the Dumlu and Kargapazarı areas) overlies the Rhodope-Pontide fragment, whereas the eastern part (i.e., the Horasan, Aladağ, and Kağızman areas, including Mount Ararat) overlies the Northwest Iranian fragment (Figs. 1 and 2). In contrast, the area south of the Aras River (i.e., a line coinciding approximately with the Erzurum-Horasan-Kağızman line) is underlain by the East Anatolian accretionary complex (EAAC, Fig. 1). The contact between the Rhodope-Pontide and the Northwest Iranian fragments may pass through the Pasinler area in a northeast-southwest direction beneath collision-related volcanic sequence. Unfortunately, these two tectonic blocks are scarcely exposed beneath the Erzurum-Kars plateau, because they are masked by a thick pile of volcanic sequence in most places. The deeper parts of the Rhodope-Pontide fragment crop out in discrete areas in the Pontides (e.g., the Pulur complex; Topuz et al., 2004) some distance from the study area, while the deeper parts of the Northwest Iranian fragment are exposed in Armenia (e.g., the Tsakhkuniats basement outcrop of the Hankavan-Takarly and the Agveran massifs; Karapetian et al., 2001). The Pulur complex is composed of a heterogeneous set of granulite-facies rocks ranging from quartz-rich mesocratic gneisses to silica- and alkali-deficient, Fe-, Mg-, and Al-rich melanocratic rocks (Topuz et al., 2004). The Tsakhkuniats basement outcrop in Armenia is also composed of a quite heterogeneous rock sequence consisting of trondhjemitic, phyillitic, albite-plagiogranitic, and plagiogranite- and granite-migmatitic lithologies (Karapetian et al., 2001). To the best of our knowledge, there are no isotopic data available from the basement of the Eastern Pontides. Isotopic data are, however, reported for the Tsakhkuniats basement outcrop (Karapetian et al., 2001) and indicate that these rocks are also heterogeneous in terms of their isotopic contents: their $^{87}Sr/^{86}Sr$ values range from 0.7038 (in trondhjemites) to 0.7222 (in phyllites).

ANALYTICAL TECHNIQUES

Because of their young age and the semiarid climate, volcanic units on the Erzurum-Kars plateau are quite fresh. Thus, element transfer due to weathering is probably not an important issue for most of the volcanics under consideration.

Radiogenic Isotope Analysis

A subset of 23 fresh representative lava samples from the Erzurum-Kars plateau was chosen for isotope analysis and provides a good temporal and spatial record of collision-related

volcanism on the plateau. These samples had previously been analyzed for major oxides and trace elements, and the results had been published (Keskin et al., 1998).

Pb, Sr, and Nd were extracted on the same dissolution using ~100–200 mg of the powder of the rock samples. After dissolution, using ~1 ml of HNO_3 combined with 3–5 ml of HF, residues were converted to nitrate and finally chloride; 1 ml of 1M HBr was then added to the residue. Pb was separated by passing the sample through columns prepared from disposable PVC pipette tips fitted with a 2-mm-diameter polyethylene frit containing Dowex 1 × 8 200–400 mesh resin; completely new columns were prepared for each sample to minimize the Pb blank. The Sr and Nd fractions were collected in 2 ml of 1M HBr and Pb collected in 1 ml of 6M HCl. Sr and Nd were purified using standard one- and two-column cation exchange techniques, respectively. Sr and Pb were run as the metal species on single Ta and single Re filaments, respectively, using a Finnegan MAT 262 multicollector mass spectrometer at the NERC Isotope Geosciences Laboratory (NIGL), UK; Nd was run as the metal species on triple Re-Ta filament assemblies using a VG354 multicollector mass spectrometer, also located at NIGL. The blanks for Sr and Pb were less than 800 pg and 250 pg, respectively. Reference standards throughout the course of analysis gave average values of $^{87}Sr/^{86}Sr$ = 0.710208 ± 44 (2σ) for the NBS987 standard, $^{143}Nd/^{144}Nd$ = 0.511109 ± 42 (2σ) for the Johnson Matthey Nd standard. $^{87}Sr/^{86}Sr$ was normalized to $^{86}Sr/^{88}Sr = 0.1194$; $^{143}Nd/^{144}Nd$ was normalized to a value of $^{146}Nd/^{144}Nd = 0.7219$. The Pb mass fractionation was 0.09% per a.m.u. Based on repeated runs of NBS981 common Pb standard, the reproducibility is better than ± 0.1%. Pb isotopic ratios were corrected relative to the average standard Pb isotopic compositions of Todt et al. (1984). Internal errors on individual isotope measurements were always much smaller than the standard reproducibility reported here; therefore, the ability to reproduce the standards should be taken as the limiting factor in interpreting the uncertainty of any given analysis. The full isotopic data set is presented as Table 1.

Oxygen ($\delta^{18}O$) Isotope Analysis

$^{18}O/^{16}O$ ratios of 11 samples were determined by a gas-source mass spectrometer at the NERC Isotope Geoscience Laboratory, British Geological Survey in Nottingham, UK. Also analyzed were the mineral separates, including 10 plagioclase, 7 amphibole, and 5 orthopyroxene separates and a biotite separate extracted from these samples by hand-picking. Whole-rock sample duplications give a mean error of ±0.3‰, comparable to the mean error of laboratory standard (basalt) duplicate pairs run at the same time (i.e., 0.2‰). The mean error also compares with secondary control determinations between analytical runs of ±0.3‰.

Electron Microprobe Analysis

Electron microprobe analyses of major elements in 57 amphibole phenocrysts from a total of 21 representative samples were performed by a Cambridge Instruments Geoscan at the University of Durham, UK, using a focused electron beam and an operation condition of 15 kV gun potential with a 70–75 μa beam current. A Co standard was used to calibrate the system. Representative analyses are presented in Table 3 later in this article.

RESULTS

Variations in Sr-Nd-Pb isotopes in each of the six subareas (see Fig. 2 for these subareas) across the Erzurum-Kars plateau are presented in Figure 5A through E, and the data are reported in Table 1. There is a systematic spatial variation in $^{206}Pb/^{204}Pb_{(i)}$ ratios, which progressively increase from 18.638 (in the Mount Dumlu area) in the west to 19.068 (in the Kağızman area) in the east. $^{143}Nd/^{144}Nd_{(i)}$ and $^{208}Pb/^{204}Pb_{(i)}$ values also tend to increase from west to east. In contrast, neither $^{87}Sr/^{86}Sr_{(i)}$ nor $^{207}Pb/^{204}Pb_{(i)}$ exhibits significant variations across the plateau (Fig. 5D). These results thus indicate that noticeable isotopic variations exist as a function of space and time in the lavas of the Erzurum-Kars plateau.

Nd-Sr Isotope Geochemistry

A Sr versus Nd isotopic plot (Fig. 6A) indicates that the majority of samples from the Erzurum-Kars plateau have radiogenic $^{87}Sr/^{86}Sr_{(i)}$ and unradiogenic $^{143}Nd/^{144}Nd_{(i)}$. They plot within the mantle array between mid-ocean ridge basalt (MORB) and bulk silicate earth (BSE).

In detail, the plateau-forming basalts of the late stage in the Horasan area and basaltic lavas of the early stage in the Mount Kargapazarı area contain the most radiogenic $^{143}Nd/^{144}Nd_{(i)}$ and unradiogenic $^{87}Sr/^{86}Sr_{(i)}$ on the plateau, and the intermediate lavas of the middle stage and late stage lavas from the Pasinler area contain the most radiogenic $^{87}Sr/^{86}Sr_{(i)}$. A lava sample from the Eocene Kışlaköy formation (i.e., MK343; see the third stratigraphic column in Fig. 2) plots in the same area as the collision-related lavas of the Erzurum-Kars plateau.

Pb Isotope Geochemistry

On the projections of $^{207}Pb/^{204}Pb_{(i)}$ versus $^{206}Pb/^{204}Pb_{(i)}$ (Fig. 7A, enlargement 7B), $^{208}Pb/^{204}Pb_{(i)}$ versus $^{206}Pb/^{204}Pb_{(i)}$ (Fig. 7C, enlargement in 7D), and $^{208}Pb/^{204}Pb_{(i)}$ versus $^{207}Pb/^{204}Pb_{(i)}$ (Fig. 7E, enlargement in 7F), all the samples from the Erzurum-Kars plateau plot above the Northern Hemisphere Reference Line (Hart, 1984). A sample (MK289) collected from the base of the volcanostratigraphic section of the Kargapazarı area plots to the left of the geochron. This may be due to the contamination of this sample by old continental crustal material. The Eocene sample, MK343, from the Pasinler area plots very close to the field of the Dumlu-Kargapazarı area, especially in $^{207}Pb/^{204}Pb_{(i)}$-$^{206}Pb/^{204}Pb_{(i)}$ space; however, its $^{208}Pb/^{204}Pb_{(i)}$

TABLE 1. Sr-Nd-Pb-O ISOTOPE ANALYSES OF REPRESENTATIVE SAMPLES FROM SIX SUBAREAS OF THE ERZURUM-KARS PLATEAU

Area	Unit	Stage	Sample	Lithology	SiO_2	LOI	Age (Ma)	$^{87}Sr/^{86}Sr$	$^{87}Sr/^{86}Sr_{(i)}$	$^{143}Nd/^{144}Nd$	$^{143}Nd/^{144}Nd_{(i)}$
Mt. Dumlu	Df	Middle	MK251	Dac	65.08	0.94	*ca. 5.5*	0.704619 ± 7	0.704593	0.512723 ± 2	0.512720
	Df	Middle	MK93	Dac	63.49	1.60	*ca. 5.5*	0.704748 ± 7	0.704717	0.512725 ± 3	0.512722
	Df	Middle	MK49	Dac	66.26	1.89	*ca. 5.5*	0.704605 ± 7	0.704556	0.512758 ± 3	0.512754
Mt. Kargapazarı	*Gof*	Middle	MK268	Dac	65.47	1.62	*ca. 6*	0.704596 ± 7	0.704524	0.512761 ± 3	0.512756
	Gunf	Middle	MK277	And	60.58	0.84	*ca. 6*	0.704355 ± 7	0.704322	0.512786 ± 3	0.512781
	Cpd	Middle	MK265	Dac	63.90	1.27	*ca. 7*	0.704583 ± 7	0.704537	0.512738 ± 3	0.512733
	Kf	Early	MK281	TrAnd	56.99	0.97	*ca. 6.7*	0.703967 ± 7	0.703931	0.512904 ± 3	0.512898
	Kf	Early	MK289	Ba	49.09	1.47	*ca. 7*	0.703910 ± 7	0.703904	0.512853 ± 4	0.512847
Pasinler	Ard	Late	MK338	Rhy	71.00	0.55	*ca. 5*	0.705400 ± 8	0.704772	0.512831 ± 4	0.512828
	Kv	Late	MK63	BaAnd	54.39	4.56	5.73 ± 0.22	0.704829 ± 7	0.704824	0.512725 ± 3	0.512721
	Kv	Late	MK101	BaAnd	57.01	1.18	*ca. 5.5*	0.704734 ± 7	0.704707	0.512754 ± 3	0.512750
	Kpd	Middle	MK112	Dac	66.81	1.81	*ca. 5.5*	0.704496 ± 7	0.704444	0.512846 ± 5	0.512842
	Bad	Early	MK117	And	62.14	0.77	7.83 ± 0.12	0.704236 ± 7	0.704188	0.512831 ± 3	0.512825
	En1	*Eocene*	MK343	BaTrAnd	54.56	3.22	38.5 ± 0.7	0.704573 ± 6	0.704330	0.512814 ± 3	0.512800
Horasan	Hpl	Late	MK130	BaTrAnd	54.36	0.14	*ca. 4.1*	0.703396 ± 6	0.703390	0.512934 ± 5	0.512930
	Hpl	Late	MK139	Ba	49.67	0.30	*ca. 4.1*	0.703708 ± 7	0.703705	0.512935 ± 3	0.512931
	Kpad	Middle	MK132	Dac	64.18	1.11	*ca. 4.1*	0.704730 ± 7	0.704709	0.512790 ± 4	0.512786
	Sd	Middle	MK154	Dac	66.91	1.13	*ca. 6*	0.704822 ± 6	0.704786	0.512727 ± 3	0.512723
	Kob	Early	MK144	Ba	48.76	2.47	11.1 ± 0.5	0.704582 ± 7	0.704570	0.512799 ± 3	0.512791
Mt. Aladağ	Af	Late	MK168	And	60.45	0.46	*ca. 3.5*	0.704053 ± 7	0.704031	0.512864 ± 2	0.512864
	Abil	Early	MK158	TrAnd	61.74	1.35	*ca. 5*	0.704523 ± 7	0.704497	0.512832 ± 4	0.512829
Kağizman	Kpf	Late	MK175	BaTrAnd	53.66	0.23	2.72 ± 0.10	0.704303 ± 6	0.704298	0.512805 ± 3	0.512803
	Pf	Early	MK174	TrDac	66.48	1.10	*ca. 5*	0.704367 ± 7	0.704297	0.512878 ± 3	0.512874

Area	Unit	Stage	Sample	Lithology	SiO_2	LOI	Age (Ma)	$^{206}Pb/^{204}Pb$	$^{206}Pb/^{204}Pb_{(i)}$	$^{207}Pb/^{204}Pb$	$^{207}Pb/^{204}Pb_{(i)}$	$^{208}Pb/^{204}Pb$	$^{208}Pb/^{204}Pb_{(i)}$	$\delta^{18}O$
Mt. Dumlu	Df	Middle	MK251	Dac	65.08	0.94	*ca. 5.5*	18.647	18.646	15.604	15.604	38.715	38.704	7.3
	Df	Middle	MK93	Dac	63.49	1.60	*ca. 5.5*	18.660	18.660	15.610	15.609	38.725	38.712	8.2
	Df	Middle	MK49	Dac	66.26	1.89	*ca. 5.5*	18.639	18.638	15.597	15.597	38.690	38.676	9.0
Mt. Kargapazarı	*Gof*	Middle	MK268	Dac	65.47	1.62	*ca. 6*	18.666	18.664	15.593	15.592	38.698	38.682	10.0 ± 0.3
	Gunf	Middle	MK277	And	60.58	0.84	*ca. 6*	18.683	18.682	15.606	15.605	38.736	38.721	7.2 ± 0.7
	Cpd	Middle	MK265	Dac	63.90	1.27	*ca. 7*	18.696	18.695	15.610	15.609	38.769	38.753	
	Kf	Early	MK281	TrAnd	56.99	0.97	*ca. 6.7*	18.735	18.734	15.604	15.603	38.764	38.748	
	Kf	Early	MK289	Ba	49.09	1.47	*ca. 7*	17.663	17.663	15.553	15.553	37.494	37.493	
Pasinler	Ard	Late	MK338	Rhy	71.00	0.55	*ca. 5*	18.943	18.942	15.621	15.621	38.918	38.897	
	Kv	Late	MK63	BaAnd	54.39	4.56	5.73 ± 0.22	18.940	18.939	15.644	15.644	38.990	38.974	
	Kv	Late	MK101	BaAnd	57.01	1.18	*ca. 5.5*	18.937	18.936	15.638	15.638	38.966	38.951	
	Kpd	Middle	MK112	Dac	66.81	1.81	*ca. 5.5*	18.798	18.797	15.614	15.613	38.834	38.823	9.4
	Bad	Early	MK117	And	62.14	0.77	7.83 ± 0.12	18.817	18.816	15.625	15.624	38.867	38.853	
	En1	*Eocene*	MK343	BaTrAnd	54.56	3.22	38.5 ± 0.7	18.625	18.624	15.605	15.604	38.593	38.539	7.5
Horasan	Hpl	Late	MK130	BaTrAnd	54.36	0.14	*ca. 4.1*	18.940	18.939	15.623	15.623	38.902	38.895	
	Hpl	Late	MK139	Ba	49.67	0.30	*ca. 4.1*	18.934	18.933	15.668	15.667	39.040	39.031	
	Kpad	Middle	MK132	Dac	64.18	1.11	*ca. 4.1*	18.946	18.944	15.626	15.625	38.926	38.910	6.5
	Sd	Middle	MK154	Dac	66.91	1.13	*ca. 6*	19.045	19.044	15.728	15.727	39.185	39.171	9.3
	Kob	Early	MK144	Ba	48.76	2.47	11.1 ± 0.5	19.024	19.022	15.665	15.664	39.075	39.053	
Mt. Aladağ	Af	Late	MK168	And	60.45	0.46	*ca. 3.5*	18.905	18.905	15.629	15.629	38.909	38.909	
	Abil	Early	MK158	TrAnd	61.74	1.35	*ca. 5*	18.989	18.988	15.619	15.619	38.936	38.928	
Kağizman	Kpf	Late	MK175	BaTrAnd	53.66	0.23	2.72 ± 0.10	19.068	19.068	15.632	15.632	38.993	38.989	
	Pf	Early	MK174	TrDac	66.48	1.10	*ca. 5*	19.030	19.029	15.617	15.616	38.985	38.973	7.3 ± 0.3

Notes: See text for analytical details. Areas and formations are as follows. *Mt. Dumlu area:* Df—the Dumlu formation (dacite/andesite). *Mt. Kargapazarı area:* Gof—the Göllerdüzü formation (dacite); Gunf—the Güngörmez formation (andesite/dacite); Cpd—the Çobandede formation (dacite); Kf—the Karapınar formation (basalt). *Pasinler area:* Ard—the Ardıçlıdağ formation (rhyolite); Kv—the Kargapazarı formation (basalt/basaltic-andesite); *Kpd*—the Kızılveren formation (dacite/andesite); Bad—the Black aphyric dacite; En1—the upper Eocene Kişlaköy volcanic member of the Narman Group. *Horasan area:* Kob—the Kötek basalt (basalt); Sd—the Saçdağ formation, south of Horasan (dacitic felsic lavas); Kpad—Köroğlu formation (dacite/andesite); Hpl—Horasan formation (plateau-forming basaltic lavas). *Mt. Aladağ area:* Af—the Aladağ formation (andesite); Abil—basal intermediate lavas (andesite/basaltic-andesite). *Kağizman area:* Kpf—the Kars plateau formation (basaltic-andesite/basalt); Pf—the Paslı formation (trachydacite). Abbreviations: And—andesite; Ba—basalt; BaAnd—basaltic-andesite; BaTrAnd—basaltic trachy-andesite; Dac—dacite; LOI—loss on ignition; Rhy—rhyolite; TrAnd—trachy-andesite; TrDac—trachy-dacite. The K/Ar ages are those presented in Keskin et al. (1998). Where no K/Ar dating was available for the sample, an approximate age estimated by volcano-stratigraphic correlations was used in the calculation of initial isotopic ratios. Approximate ages are presented in italics. For the locations of samples, see Figure 2.

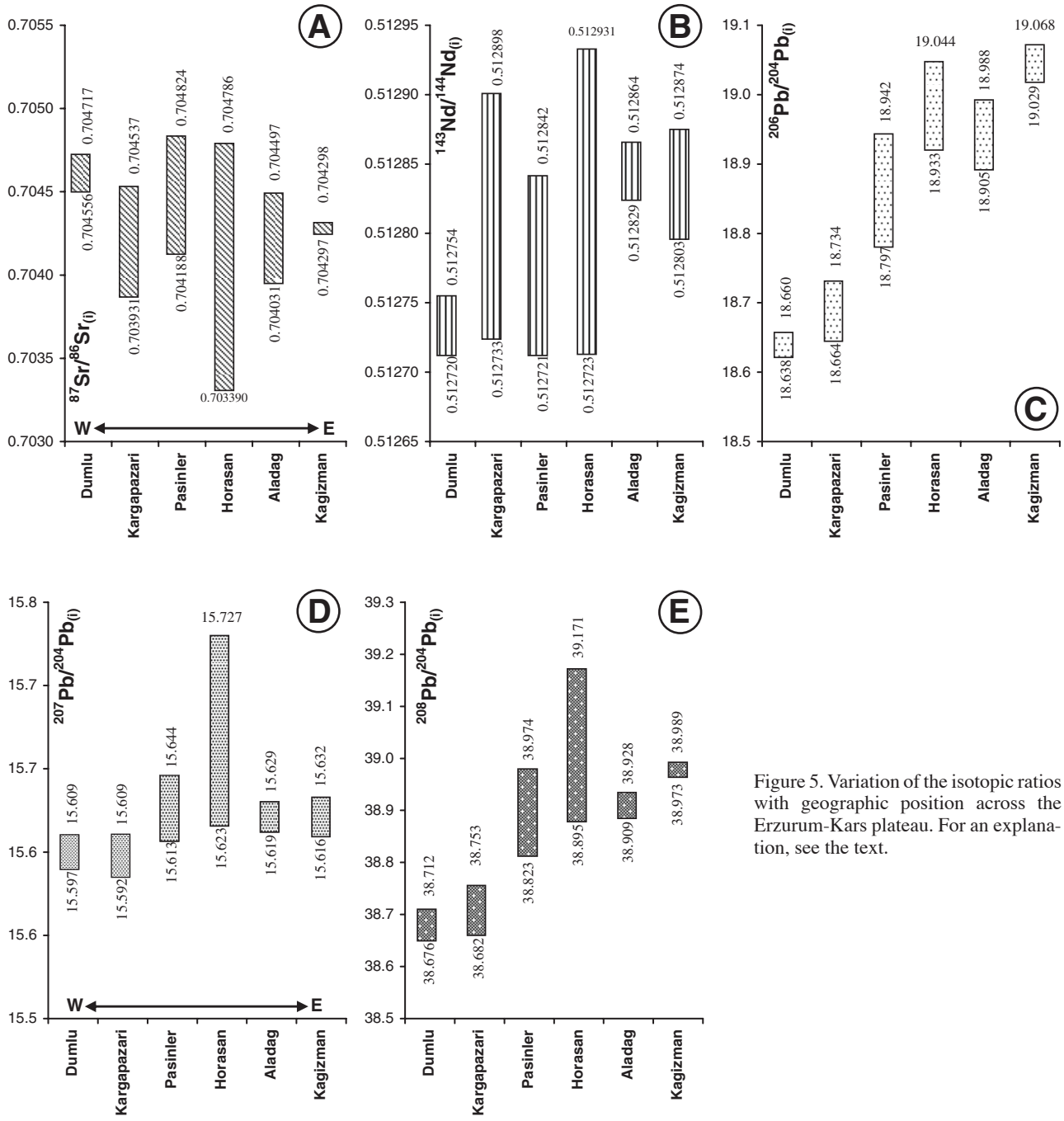

Figure 5. Variation of the isotopic ratios with geographic position across the Erzurum-Kars plateau. For an explanation, see the text.

content is much lower than that of the lavas of the Erzurum-Kars plateau.

In the enlarged plots, the lavas of the Mount Dumlu and Kargapazarı areas in the western part of the Erzurum-Kars plateau exhibit limited variation in their $^{207}Pb/^{204}Pb_{(i)}$ (15.592–15.609), $^{208}Pb/^{204}Pb_{(i)}$ (38.676–38.753), and $^{206}Pb/^{204}Pb_{(i)}$ (18.638–18.734) compositions in comparison with more radiogenic lavas of the Horasan and Kağızman areas in the eastern part of the Erzurum-Kars plateau. Lavas from the Pasinler area are transitional between the western part of the plateau and the eastern part, consistent with the geographic position of this subarea on the plateau. Lavas from the Horasan, Kağızman, and Pasinler areas display some overlap with the EMII (enriched mantle type II; Zindler and Hart, 1986) field.

There are two arrays with different gradients on the Pb-Pb plots: (1) the Horasan-Kağızman trend (in the eastern part of the

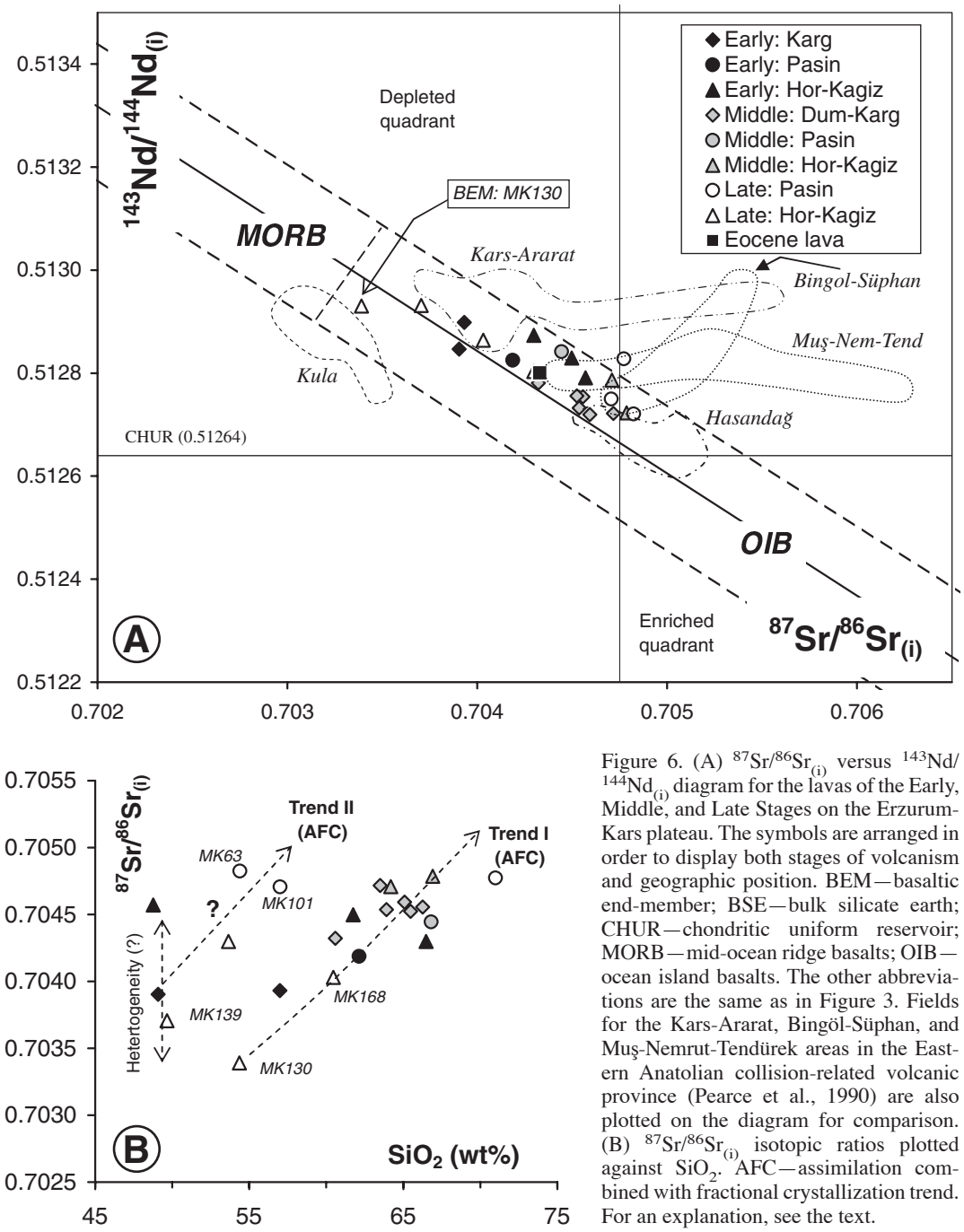

Figure 6. (A) $^{87}Sr/^{86}Sr_{(i)}$ versus $^{143}Nd/^{144}Nd_{(i)}$ diagram for the lavas of the Early, Middle, and Late Stages on the Erzurum-Kars plateau. The symbols are arranged in order to display both stages of volcanism and geographic position. BEM—basaltic end-member; BSE—bulk silicate earth; CHUR—chondritic uniform reservoir; MORB—mid-ocean ridge basalts; OIB—ocean island basalts. The other abbreviations are the same as in Figure 3. Fields for the Kars-Ararat, Bingöl-Süphan, and Muş-Nemrut-Tendürek areas in the Eastern Anatolian collision-related volcanic province (Pearce et al., 1990) are also plotted on the diagram for comparison. (B) $^{87}Sr/^{86}Sr_{(i)}$ isotopic ratios plotted against SiO_2. AFC—assimilation combined with fractional crystallization trend. For an explanation, see the text.

Erzurum-Kars plateau), and (2) the Dumlu-Kargapazarı trend (in the western part of the plateau) (Fig. 7B, D, and F). The most primitive lava sample on the plateau (i.e., BEM, MK130) plots at the junction of these two diverging trends (Fig. 7B, D, and F). Late stage lavas from the Pasinler area plot within the same field as those from the Horasan-Kağızman area, whereas early- and middle-stage lavas of the same area plot in the field occupied by the lavas of the Dumlu and Kargapazarı areas. Lavas forming the Horasan-Kağızman trend display a narrower variation in $^{206}Pb/^{204}Pb_{(i)}$ but a wider variation in $^{207}Pb/^{204}Pb_{(i)}$ than those of the Dumlu-Kargapazarı trend. Interestingly, lavas from the Kula area in western Turkey (Alıcı et al., 2002) and the Hasandağ area in central Anatolia (Deniel et al., 1998) resemble lavas from the Dumlu-Kargapazarı and the Horasan-Kağızman areas, respectively, in $^{207}Pb/^{204}Pb_{(i)}$-$^{206}Pb/^{204}Pb_{(i)}$ and $^{208}Pb/^{204}Pb_{(i)}$-$^{207}Pb/^{204}Pb_{(i)}$ space (though with a small shift). How-

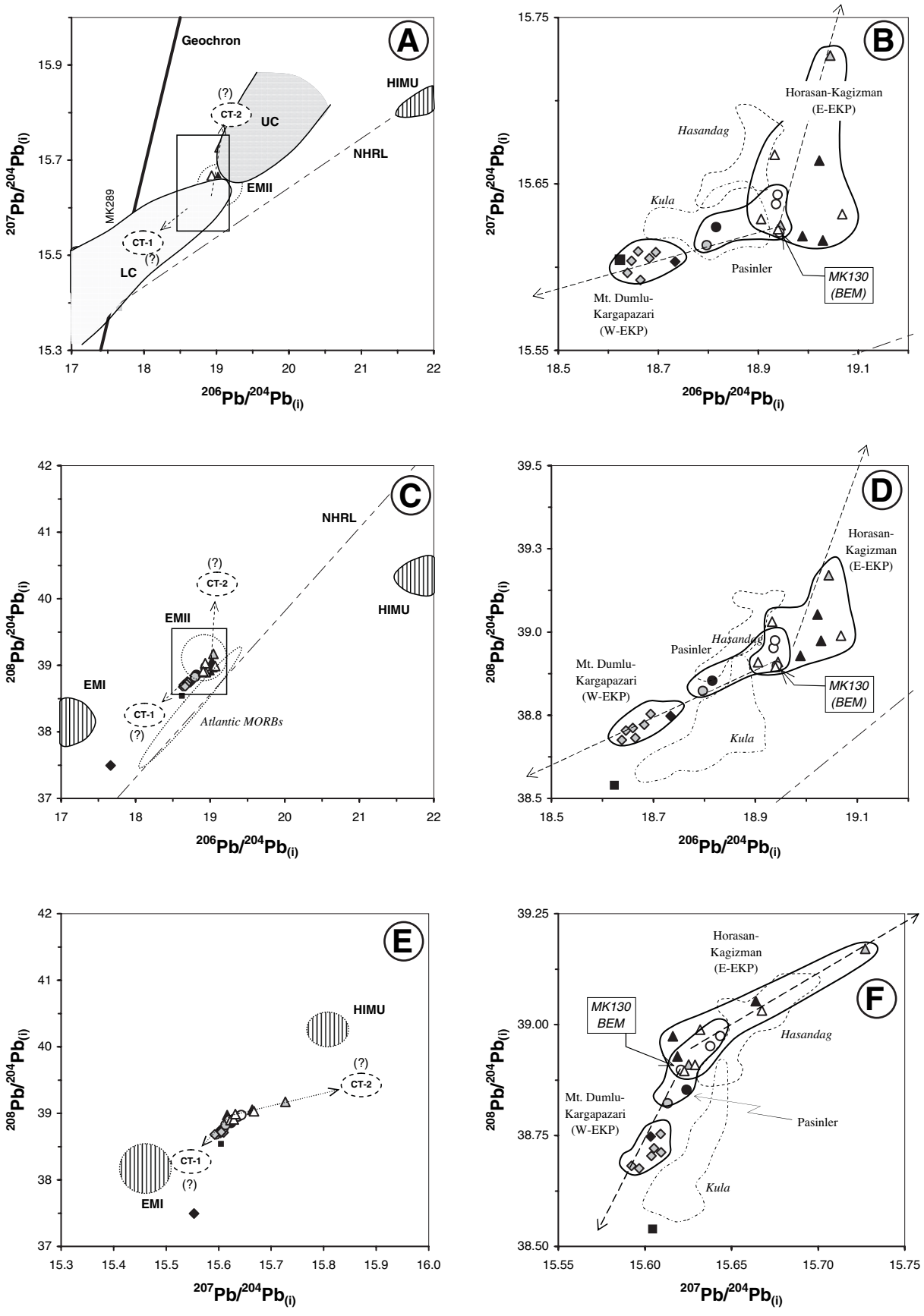

ever, such a similarity is not apparent in $^{207}Pb/^{204}Pb_{(i)}$-$^{206}Pb/^{204}Pb_{(i)}$ space.

Oxygen Isotope Variations

The $\delta^{18}O$ values of the lava samples and the mineral separates (i.e., plagioclase, amphibole, orthopyroxene, and biotite) obtained from these samples are listed in Table 2. The $\delta^{18}O$ values of the whole-rock samples range from +6.5‰ to +10‰, while those of plagioclase, amphibole and orthopyroxene vary between +5.6‰ and +8.4‰, +6‰ and +7.7‰, and +5.1‰ and +6.7‰, respectively (Table 2). Except for one orthopyroxene sample with exceptionally low $\delta^{18}O$ (5.1‰, MK132), all the analyzed samples have $\delta^{18}O$ values between 6 and 8.4, which is within the normal range for unaltered igneous rocks (Taylor, 1968). Differences in whole-rock–mineral $\delta^{18}O$ values ($\Delta^{18}O_{WR\text{-}mineral}$) and fractionation values between various minerals (e.g., $\Delta^{18}O_{Plg\text{-}Amp}$) are also presented in Table 2. $\Delta^{18}O_{WR\text{-}mineral}$ values vary between –0.1‰ (plg) and +3.4‰ (opx), averaging +1.4‰. The spread in magmatic $\delta^{18}O$ for plagioclase, amphibole, and orthopyroxene is 2.8‰, 1.7‰, and 1.6‰, respectively. Seven plagioclase-amphibole pairs yielded a fractionation of 0.55‰ ± 0.26‰ (1σ). Five plagioclase-orthopyroxene pairs produced a fractionation of 0.96‰ ± 0.55‰ (1σ). The $\Delta^{18}O_{Amp\text{-}Opx}$ is around 0.81‰ ± 0.6‰ (Table 2).

INTERPRETATION OF THE GEOCHEMICAL DATA

Sr-Nd Isotope Systematics

On the plot of $^{87}Sr/^{86}Sr_{(i)}$ versus SiO_2 (Fig. 6B), two separate trends may be identified. Although $^{87}Sr/^{86}Sr$ values vary in a relatively narrow range, between 0.703390 and 0.704824, they display a significant linear correlation with SiO_2 along these two inferred trends (trends I and II). Trend II is formed only by the lavas of the late stage and has the higher Sr isotope ratio for a given silica content, indicating a more enriched basaltic end-member. Trend I, on the other hand, is formed by the lavas from all three stages. The correlation between $^{87}Sr/^{86}Sr_{(i)}$ and SiO_2 indicates that assimilation of crustal material combined with fractional crystallization (i.e., AFC) may have operated during the magma chamber evolution of these lavas (Fig. 6B). This is consistent with the results of the AFC model presented by Keskin et al. (1998).

As stated earlier, lavas of the Horasan, Kağızman, and Pasinler areas display some overlap with the EMII field (Zindler and Hart, 1986). However, the EMII field is located far away from the lavas of the Erzurum-Kars plateau on both $^{87}Sr/^{86}Sr_{(i)}$ versus $^{206}Pb/^{204}Pb_{(i)}$ and $^{143}Nd/^{144}Nd_{(i)}$ versus $^{206}Pb/^{204}Pb_{(i)}$ plots (not shown), because lavas of the plateau are much more enriched in $^{87}Sr/^{86}Sr_{(i)}$ than the EMII component. Therefore, we argue that the isotopic variations in the lavas of the Erzurum-Kars plateau could not be associated with the EMII end-member.

Pb Isotope Systematics

Variations in Pb isotopic ratios within the continental crust can be used as a powerful tool in the identification of crustal reservoirs or regional domains. The aforementioned variations may also be useful for determining the isotopic compositions of lead in subducted sediments. Moreover, distinct Pb isotope signatures can be utilized as geochemical tracers, because they reflect the crustal material involved in magma genesis by means of assimilation, crustal melting (Zartman, 1974; Wörner et al., 1992), and source contamination.

As described previously, two distinct trends diverging from a common basic magma composition (i.e., sample MK130) exist on the Pb-Pb plots (Fig. 7). These two trends may be interpreted as mixing lines between a common primitive basaltic magma (i.e., BEM) composition and two contrasting end-member compositions. Although the Dumlu-Kargapazarı trend points toward the EMI field (Zindler and Hart, 1986) in $^{207}Pb/^{204}Pb_{(i)}$-$^{206}Pb/^{204}Pb_{(i)}$ space, a similar relationship is not seen in the $^{87}Sr/^{86}Sr_{(i)}$ versus $^{206}Pb/^{204}Pb_{(i)}$ and the $^{143}Nd/^{144}Nd_{(i)}$ versus $^{206}Pb/^{204}Pb_{(i)}$ plots (not shown). Therefore, we argue that this relationship cannot be linked to the EMI mantle source.

On a plot of $^{206}Pb/^{204}Pb_{(i)}$ versus SiO_2 (Fig. 8), the lavas from the western part of the Erzurum-Kars plateau and those in the eastern part plot in two distinct fields, which form two diverging trends: (1) a Dumlu-Kargapazarı trend of decreasing $^{206}Pb/^{204}Pb_{(i)}$ with increasing SiO_2 and (2) a less coherent Horasan-Kağızman trend of nearly constant $^{206}Pb/^{204}Pb_{(i)}$. Lavas from the Pasinler area are scattered between these two fields. Note that both of these trends contain lavas from all three volcanic stages (i.e., the early, middle, and late stages). Therefore, we argue that the covariation between $^{206}Pb/^{204}Pb_{(i)}$ and SiO_2 is linked to the AFC process, whereas the presence of separate trends reflects differences in Pb isotopic composition of the crustal material assimilated across the Erzurum-Kars plateau. In this case, these two contrasting mixing end-members may correspond to two different crustal compositions.

Figure 7. $^{207}Pb/^{204}Pb_{(i)}$ (A, B) and $^{208}Pb/^{204}Pb_{(i)}$ (C, D) versus $^{206}Pb/^{204}Pb_{(i)}$ and $^{208}Pb/^{204}Pb$ (E, F) versus $^{207}Pb/^{204}Pb_{(i)}$ diagrams for the lavas of the Erzurum-Kars plateau (EKP), providing evidence for two distinct assimilation trends. The symbols are as in Figures 3 and 6. Fields of Hasandag (city of Aksaray, Central Anatolia: Deniel et al., 1998) and Kula (city of Manisa, Aegean region of Western Turkey: Alıcı et al., 2002) are shown for comparison. Note that these two areas are the only places in Turkey from which Pb isotopic data are available. BEM—basaltic end-member; CT-1—crust type 1 = hypothetical lower-crustal composition; CT-2—crust type 2 = hypothetical upper-crustal composition (Zindler and Hart, 1986); EMI—enriched mantle type I (Zindler and Hart, 1986); HIMU—HIgh MU (MU = μ = $^{238}U/^{204}Pb$ (Lustrino and Dallai, 2003); EMII—enriched mantle type II (enriched in Sr); LC—lower crust; NHRL—Northern Hemisphere Reference Line (Hart, 1984); UC—upper crust.

TABLE 2. THE $\delta^{18}O$ VALUES OF WHOLE ROCKS AND MINERAL SEPARATES, THE Δ VALUES BETWEEN WHOLE ROCKS AND MINERAL PAIRS, AND THE CALCULATED $\delta^{18}O_{MELT}$ AND MEAN CRYSTAL-MELT FRACTIONATION VALUES

Sample no	Area	Stage	SiO_2 (WR)	LOI	$\delta^{18}O_{WR}$ (‰ SMOW)	$\delta^{18}O_{Plag}$ (‰ SMOW)	$\delta^{18}O_{Amp}$ (‰ SMOW)	$\delta^{18}O_{Opx}$ (‰ SMOW)	$\delta^{18}O_{Bio}$ (‰ SMOW)	$\Delta_{WR\text{-}plag}$ (‰)	$\Delta_{WR\text{-}amp}$ (‰)	$\Delta_{WR\text{-}opx}$ (‰)	$\Delta_{WR\text{-}bio}$ (‰)	$\Delta_{Plg\text{-}Amp}$ (‰)	$\Delta_{Plg\text{-}Opx}$ (‰)	$\Delta_{Amp\text{-}Opx}$ (‰)
MK49	Dumlu	Middle	66.26	1.89	9.00	8.40	7.70			0.60	1.30			0.70		
MK93	Dumlu	Middle	63.49	1.60	8.20	7.35	6.70	6.03		0.85	1.50	2.17		0.65	1.32	0.67
MK251	Dumlu	Middle	65.08	0.94	7.30	7.40		6.30		–0.10		1.00			1.10	
MK277	Kargapazarı	Middle	60.58	0.84	7.20	6.70		6.70		0.50		0.50			0.00	
MK268	Kargapazarı	Middle	65.47	1.62	10.00	8.30	7.20			1.70	2.80			1.10		
MK112	Pasinler	Middle	66.81	1.81	9.40	7.90	6.90	6.03		1.50	2.50	3.37		1.00	1.87	0.87
MK338	Pasinler	Late	71.00	0.55		7.35										
MK154	S of Horasan	Middle	66.91	1.13	9.30	7.70	6.80		6.20	1.60	2.50		3.10	0.90		
MK132	N of Horasan	Middle	64.18	1.11	6.50	5.60	6.00	5.10		0.90	0.50	1.40		–0.40	0.50	0.90
MK174	Kağızman	Early	66.48	1.10	7.30	6.80	6.90			0.50	0.40			–0.10		
		Maximum value		1.89	10.00	8.40	7.70	6.70		1.70	2.80	3.37		1.10	1.87	0.90
		Minimum value		0.55	6.50	5.60	6.00	5.10		–0.10	0.40	0.50		–0.40	0.00	0.67
		Variability range		1.33	3.50	2.80	1.70	1.60		1.80	2.40	2.87		1.50	1.87	0.23
		Average		1.26	8.24	7.35	6.89	6.03		0.89	1.64	1.69		0.55	0.96	0.81
												Standard error		0.26	0.55	0.60

				Modal % of the minerals									
Sample no	Area	Stage	$\delta^{18}O_{WR}$ (‰ SMOW)	Plg (%)	Amp (%)	Opx (%)	Bio (%)	Groundmass	Calculated $\delta^{18}O_{matrix(-magma)}$	$\Delta_{magma\text{-}plag}$ (‰)	$\Delta_{magma\text{-}amp}$ (‰)	$\Delta_{magma\text{-}opx}$ (‰)	$\Delta_{magma\text{-}bio}$ (‰)
MK49	Dumlu	Middle	9.00	10.00	7.17			82.83	9.18	0.78	1.48		
MK93	Dumlu	Middle	8.20	12.67	2.83	0.83		83.67	8.40	1.05	1.70	2.37	
MK251	Dumlu	Middle	7.30	11.33	2.17	1.67		84.83	7.49	0.09		1.19	
MK277	Kargapazarı	Middle	7.20	13.83		2.83		83.34	7.30	0.60		0.60	
MK268	Kargapazarı	Middle	10.00	16.00	3.00			81.00	10.44	2.14	3.24		
MK112	Pasinler	Middle	9.40	15.00	3.00	0.50		81.50	9.79	1.89	2.89	3.76	
MK338	Pasinler	Late		12.70				87.30					
MK154	S of Horasan	Middle	9.30	9.67	3.33		0.83	86.17	9.61	1.91	2.81	9.61	3.41
MK132	N of Horasan	Middle	6.50	15.83	2.33	3.00		78.84	6.75	1.15	0.75	1.65	
MK174	Kağızman	Early	7.30	9.83	2.17			88.00	7.37	0.57	0.47	7.37	
		Maximum value		16.00	7.17	3.00	0.83	88.00	10.44	2.14	3.24	9.61	
		Minimum value		9.67	2.17	0.50	0.83	78.84	6.75	0.09	0.47	0.60	
		Range		6.33	5.00	2.50	0.00	9.16	3.69	2.05	2.77	9.01	
		Average		12.69	3.25	1.77	0.83	83.75	8.48	1.13	1.90	3.79	

$\Delta_{cryst\text{-}melt} = -1.5384$

Notes: See text for details. Abbreviations: WR—whole rock; SMOW—standard mean ocean water; plag—plagioclase; amp—amphibole; opx—orthopyroxene; bio—biotite; LOI—loss on ignition.

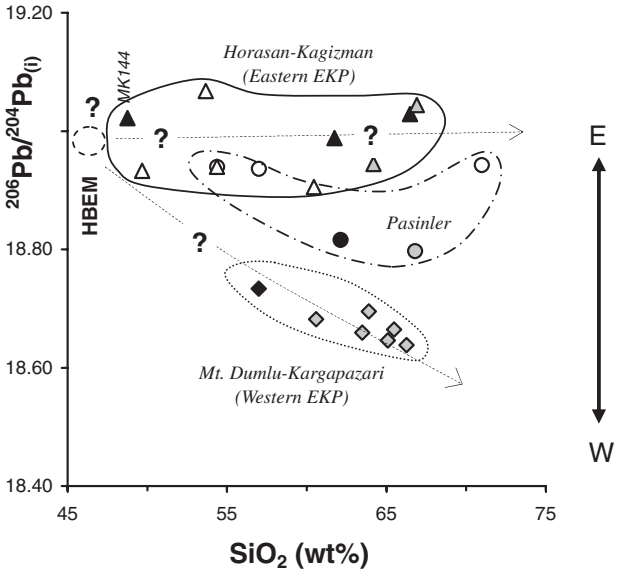

Figure 8. $^{206}Pb/^{204}Pb_{(i)}$ isotopic ratios plotted against SiO_2. The symbols are as in Figures 3 and 6. HBEM—hypothetical basaltic end-member composition from which lavas of the Erzurum-Kars plateau (EKP) are thought to have been derived.

Figure 8 also indicates that the variations in Pb isotopic ratios are spatial in nature, not temporal. We argue that Pb isotope variations should not be related to source contamination, because their relationship to $\delta^{18}O$ does not support a model that involves addition of sedimentary material to the mantle source region by subduction (see Fig. 10F later in this article). Given the lack of information for defining the precise compositions of these two end-members (there are no published isotopic data on crustal compositions from the Pontides and eastern Anatolia), we have arbitrarily marked two different crustal compositions in Figure 7A, C, and E and named them CT-1 and CT-2 (i.e., crust type 1 and crust type 2, respectively). Note that CT-2 plots somewhere close to the average upper-crustal composition, while CT-1 falls into the middle range of the average lower-crustal composition in $^{207}Pb/^{204}Pb_{(i)}$-$^{206}Pb/^{204}Pb_{(i)}$ space (Fig. 7A).

$\delta^{18}O$ Isotope Systematics

Assessing the Isotopic Equilibrium of Oxygen. In order to examine the isotopic equilibrium between mineral pairs, we constructed a bivariate plot with the axis represented by the A parameter and the term [1000 ln $\alpha_{(Plg\text{-}min)}$ – B], as proposed by Javoy et al. (1970) (Fig. 9A). We calculated a set of isotherms for a range of temperatures (i.e., from 500 to 950 °C), then plotted the values for sets of mineral pairs. On such a diagram, minerals from the same sample that are in isotopic equilibrium form a tie-line parallel to the isotherms (Rollinson, 1993). The plotted compositions imply that the isotopic compositions of plagioclases are not in equilibrium with those of orthopyroxenes (Fig. 9A).

When petrographically examined, the samples do not show evidence of hydrothermal alteration or devitrification. In order to understand the extent to which such alteration influenced the stable isotope chemistry of the rocks analyzed, we have plotted the $\delta^{18}O$ values of whole-rock and mineral separates against loss on ignition (LOI) values of the whole-rock samples in Figure 9B (see Table 1 for the LOI values). Although the $\delta^{18}O_{WR}$, $\delta^{18}O_{Plg}$, and $\delta^{18}O_{Amp}$ values increase with increasing LOI values, the correlation coefficients are low ($R^2 = 0.5$ for rock samples, 0.3 for Plg, and 0.4 for Amp) and significant only just at or below the 95% confidence level. On the other hand, SiO_2 (i.e., the measured values) and Rb, which are used as a fractionation index, also display positive correlations with the LOI values (not shown).

These relationships bring into question whether they reflect isotopic exchange between the minerals and an externally derived fluid (e.g., hydrothermal alteration). In order to assess this, we plotted the δ values of amphibole, orthopyroxene, and biotite separates against their coexisting plagioclase separates in Figure 9C. In theory, mineral-plagioclase pairs that plot with a slope of unity are presumed to be in equilibrium, whereas those deviating significantly from this slope are assumed to be in isotopic disequilibrium with each other. Only three samples (i.e., MK132, MK93, and MK174) plot off the 45° trend formed by most samples and just outside the expected fractionation range (Fig. 9C). The diagram, therefore, implies that isotopic exchange with an externally derived fluid is not important for most, if not all, samples under consideration.

Whole-Rock $\delta^{18}O$ Variations with Radiogenic Isotopic Ratios. Having concluded that variations in oxygen isotopic ratios have not been modified by alteration by externally derived fluids and that most mineral pairs are in isotopic equilibrium with each other, in this section we focus on the $\delta^{18}O$ systematics of whole-rock samples. $^{87}Sr/^{86}Sr_{(i)}$ and $^{143}Nd/^{144}Nd_{(i)}$ iso-

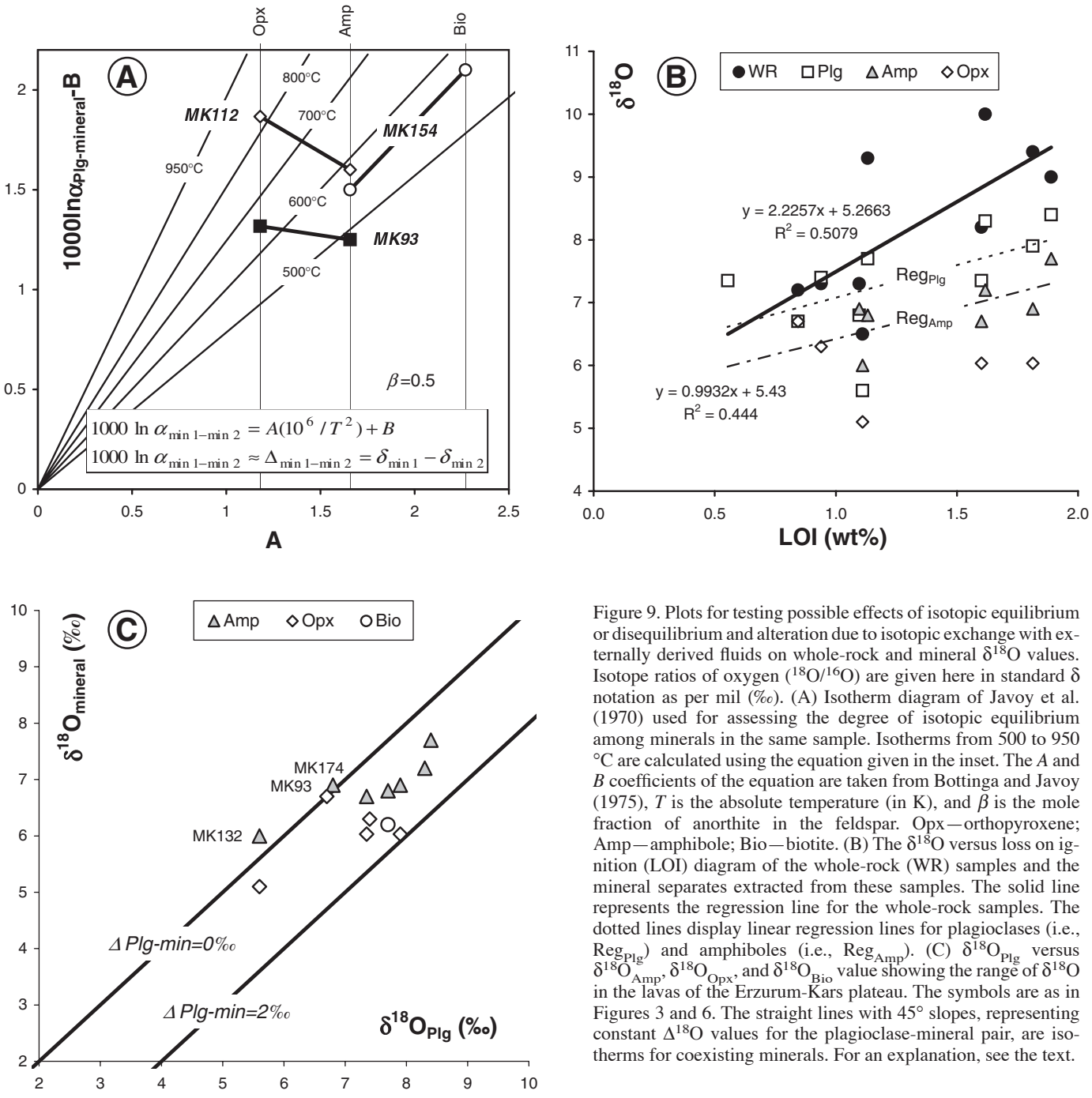

Figure 9. Plots for testing possible effects of isotopic equilibrium or disequilibrium and alteration due to isotopic exchange with externally derived fluids on whole-rock and mineral $\delta^{18}O$ values. Isotope ratios of oxygen ($^{18}O/^{16}O$) are given here in standard δ notation as per mil (‰). (A) Isotherm diagram of Javoy et al. (1970) used for assessing the degree of isotopic equilibrium among minerals in the same sample. Isotherms from 500 to 950 °C are calculated using the equation given in the inset. The *A* and *B* coefficients of the equation are taken from Bottinga and Javoy (1975), *T* is the absolute temperature (in K), and β is the mole fraction of anorthite in the feldspar. Opx—orthopyroxene; Amp—amphibole; Bio—biotite. (B) The $\delta^{18}O$ versus loss on ignition (LOI) diagram of the whole-rock (WR) samples and the mineral separates extracted from these samples. The solid line represents the regression line for the whole-rock samples. The dotted lines display linear regression lines for plagioclases (i.e., Reg_{Plg}) and amphiboles (i.e., Reg_{Amp}). (C) $\delta^{18}O_{Plg}$ versus $\delta^{18}O_{Amp}$, $\delta^{18}O_{Opx}$, and $\delta^{18}O_{Bio}$ value showing the range of $\delta^{18}O$ in the lavas of the Erzurum-Kars plateau. The symbols are as in Figures 3 and 6. The straight lines with 45° slopes, representing constant $\Delta^{18}O$ values for the plagioclase-mineral pair, are isotherms for coexisting minerals. For an explanation, see the text.

topic ratios form subvertical trends against $\delta^{18}O$ with some scatter (Fig. 10B and C). $^{87}Sr/^{86}Sr_{(i)}$ values increase slightly with increasing $\delta^{18}O$, whereas $^{143}Nd/^{144}Nd_{(i)}$ ratios decrease with increasing $\delta^{18}O$. When $^{206}Pb/^{204}Pb_{(i)}$ and $^{208}Pb/^{204}Pb_{(i)}$ are plotted against $\delta^{18}O$ (Fig. 10D and E), they align along two separate trends emanating from a common primitive basaltic composition similar to that of MK130 (i.e., BEM) and diverging from each other, possibly heading toward two different mixing end-member compositions (i.e., hypothetical crustal compositions of CT-1 and CT-2). Geographic position again probably controls the distribution of data points on this diagram: lavas in the western part of the Erzurum-Kars plateau (i.e., Mount Dumlu–Kargapazarı) are more unradiogenic than those of the eastern part (i.e., the Horasan, Aladağ, and Kağızman areas) in terms of their Pb isotope compositions, and a sample from the Pasinler area is located between these two groups. Unfortunately, no

oxygen isotope analysis for MK130 is available; therefore, we attempted to plot an approximate basic end-member composition (i.e., BEM) in Figure 10E by taking the average $\delta^{18}O$ composition of unmodified mantle-derived primitive melts (~5.5‰) into account. Because Pb isotopic ratios display two distinct linear arrays with $\delta^{18}O$, we argue that these arrays can be explained by the contamination of a primitive magma by two different hypothetical end-member compositions: CT-1 and CT-2 (see also Fig. 10).

To better define the nature of the process(es) responsible for the formation of these two trends in the lavas of the Erzurum-Kars plateau, in Figure 10F we plot theoretical trends that reflect three possible mixing models: (1) simple bulk mixing between a mantle-derived magma and two different crustal compositions, (2) contamination of a primitive magma by a crustal material through the AFC process, and (3) introduction of the crustal or sedimentary contaminant to the source prior to partial melting. Because the trends are linear, we argue that simple bulk mixing between a mantle-derived magma and crustal material, possibly as part of the AFC process, might have been responsible for the formation of these trends. Note that the crustal material underlying the western part of the Erzurum-Kars plateau around Mount Dumlu and Kargapazarı (i.e., CT-1) is much more unradiogenic than the one that underlies the eastern part of the plateau around the Horasan, Aladağ, and Kağızman areas (i.e., CT-2). However, both CT-1 and CT-2 may have similar $\delta^{18}O$ contents.

Petrologic Modeling

O Isotope Fractionation versus AFC Processes. In accordance with the behavior of $^{87}Sr/^{86}Sr_{(i)}$, the $\delta^{18}O$ values of the lavas from the Erzurum-Kars plateau increase with increasing SiO_2 (Fig. 10A) and also with a number of incompatible elements (e.g., Rb and Th), which can be considered indexes of differentiation (Fig. 11; Th is not shown). This confirms that the AFC and O isotope fractionation processes may have been important during the magma chamber evolution of the lavas on the plateau. $\delta^{18}O$ exhibits a much greater variation (between 6.5‰ and 10‰) than $^{87}Sr/^{86}Sr$. $\delta^{18}O$ is around 5.5‰ in mantle-derived magmas (<6‰ according to Kyser, 1986) that have not experienced fractionation and/or crustal assimilation and ~19‰ in isotopically evolved upper crust (Harmon et al., 1981). Therefore, significant AFC and/or isotopic fractionation are needed to produce $\delta^{18}O$ values as high as 10‰ (Fig. 10A). At this point, it is important to evaluate the relative importance of AFC for a better understanding of the magma evolution on the Erzurum-Kars plateau and the degree of magma-crust interaction.

Modeling Oxygen Isotope Fractionation. The value of the solid-magma O isotope fractionation factor (α) is the key parameter for modeling O isotope fractionation. In order to calculate the value of α, we first calculated $\delta^{18}O$ values for the melt by utilizing $\delta^{18}O$ values of whole-rock and mineral separates as well as modal percentages of these separates. We then calculated a mean mineral-melt fractionation factor ($\Delta_{mineral\text{-}melt}$) of –1.54‰ using the $\delta_{mineral\text{-}melt}$ values and the modal percentages of each mineral (see Table 2). Finally, we used equation 2 (given in the inset of Fig. 11A) to calculate a mineral-magma $\delta^{18}O$ fractionation factor (i.e., α) of 0.99846 from the calculated mean $\Delta_{mineral\text{-}melt}$ value.

Rb is highly incompatible during the crystallization of either anhydrous or hydrous phases at basic to intermediate magma compositions, except in the most acid magmas that experience biotite fractionation. The Harker diagram of Rb versus SiO_2 (see Fig. 5B *in* Keskin et al., 1998) displays a positive trend at basic to intermediate compositions until SiO_2 reaches 74 wt%. This indicates that biotite was not an important fractionating phase in the Erzurum-Kars plateau volcanics; hence, Rb is a suitable fractionation index for modeling the fractional crystallization (FC) process. In order to examine the extent to which FC is responsible for the observed positive correlation between Rb and $\delta^{18}O$, we modeled a set of FC vectors for a set of mineral-melt $\delta^{18}O$ fractionation factors (i.e., α values) ranging from +0.4‰ to –1‰ and then plotted them against Rb in Figure 11A. We selected MK130 as the basic end-member in the diagram (Fig. 11A), because it is one of the most primitive samples on the Erzurum-Kars plateau. The FC paths on the diagram represent the trends that could be expected for closed-system crystal fractionation from a calc-alkaline magma.

In Figure 11A, the samples with $\delta^{18}O$ values of less than +7.3‰ (i.e., MK132, MK174, MK277, and MK251) plot around or very close to the modeled fractionation vectors, indicating that differentiation through closed-system fractionation with or without assimilation may account for the O isotope variations of these samples. Apart from these four samples, the data points plot away from FC curves toward much higher $\delta^{18}O$ values. It is evident from the graph that fractionation cannot generate such an increase in $\delta^{18}O$. Therefore, we argue that AFC may indeed account for most, if not all, of the Sr and O isotopic variations in the lavas of the Erzurum-Kars plateau. In the next section, we focus on the modeling of the AFC process by utilizing $\delta^{18}O$ and Rb values.

Modeling the AFC Process. Because of the large contrast between $\delta^{18}O$ contents of the continental upper crust (~+19‰; Harmon et al., 1981) and those of the mantle-derived melts (~+5.5‰), $\delta^{18}O$ values are useful for estimating the degree of assimilation. However, it should be noted that oxygen isotopes are insensitive to small degrees of assimilation, because oxygen makes up around 50% of the mass of volcanic rocks. The AFC modeling has been conducted using the AFC equations of De Paolo (1981), the bulk partition coefficient (D) and O fractionation (Δ) values presented in the inset of Figure 11B, a parental magma corresponding to the basalt sample MK130, and the average upper-crustal composition of Taylor and McLennan (1985). The $\delta^{18}O$ value of the upper crust (i.e., +19‰) is that for isotopically evolved continental crust of Harmon et al. (1981). Note that magma compositions for different degrees of fractional crystallization can be modeled for different values of *r* (the ratio of the rate of assimilation to the rate of fractional crys-

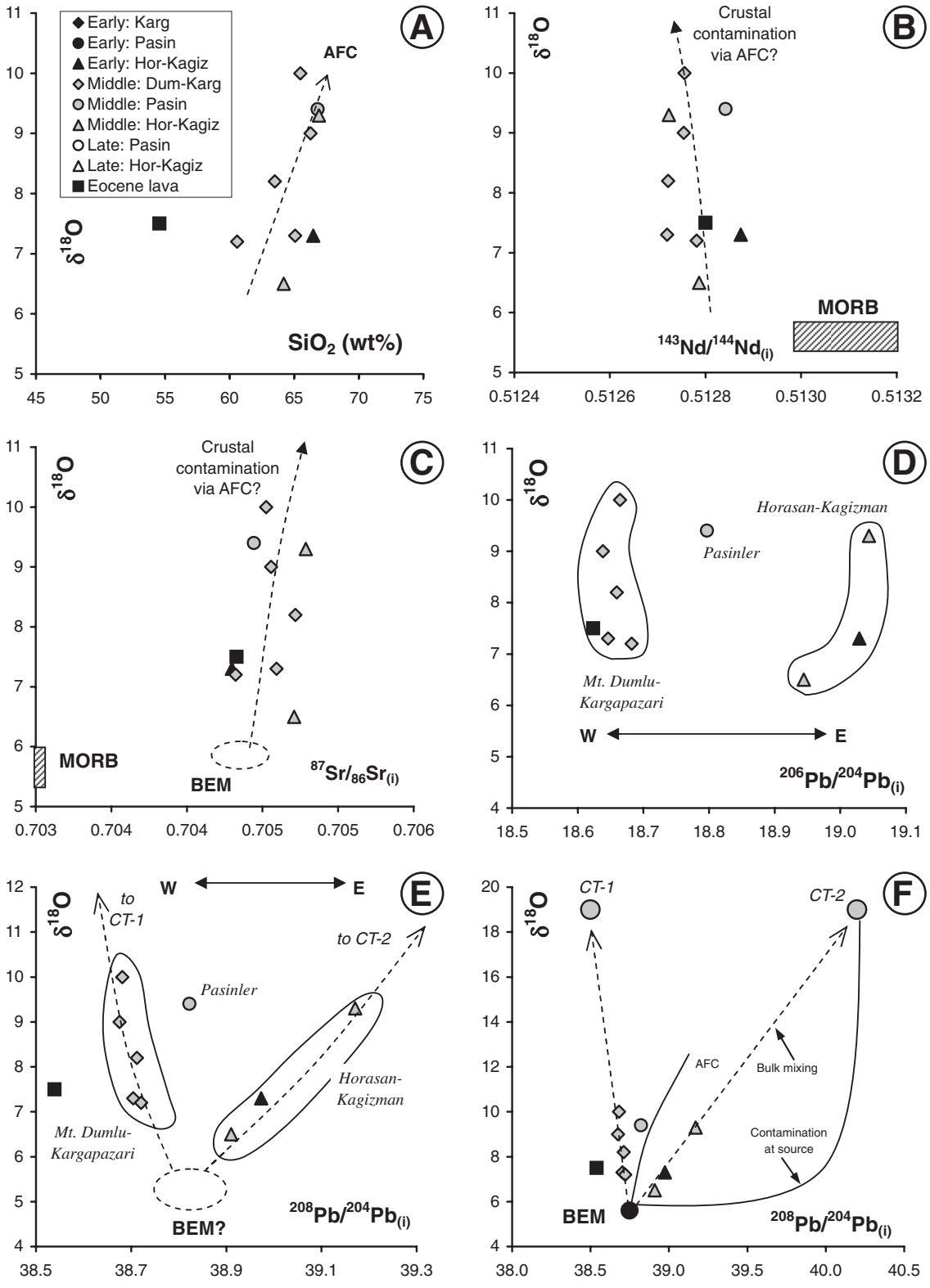

Figure 10. $\delta^{18}O$ values of the Erzurum-Kars plateau samples plotted against their (A) SiO_2 values, (B) $^{143}Nd/^{144}Nd_{(i)}$, (C) $^{87}Sr/^{86}Sr_{(i)}$, (D) $^{206}Pb/^{204}Pb_{(i)}$, and (E) $^{208}Pb/^{204}Pb_{(i)}$. (F) $\delta^{18}O$ versus $^{208}Pb/^{204}Pb_{(i)}$ diagram displaying hypothetical curves between a primitive magma composition and two different end-member compositions (i.e., CT-1 and CT-2) for simple bulk mixing, assimilation and fractional crystallization (AFC), and source contamination. The symbols are as in Figures 3 and 6. BEM—basaltic end-member; CT-1—crust type 1; CT-2—crust type 2; MORB—mid-ocean ridge basalts. For more explanation, see the text.

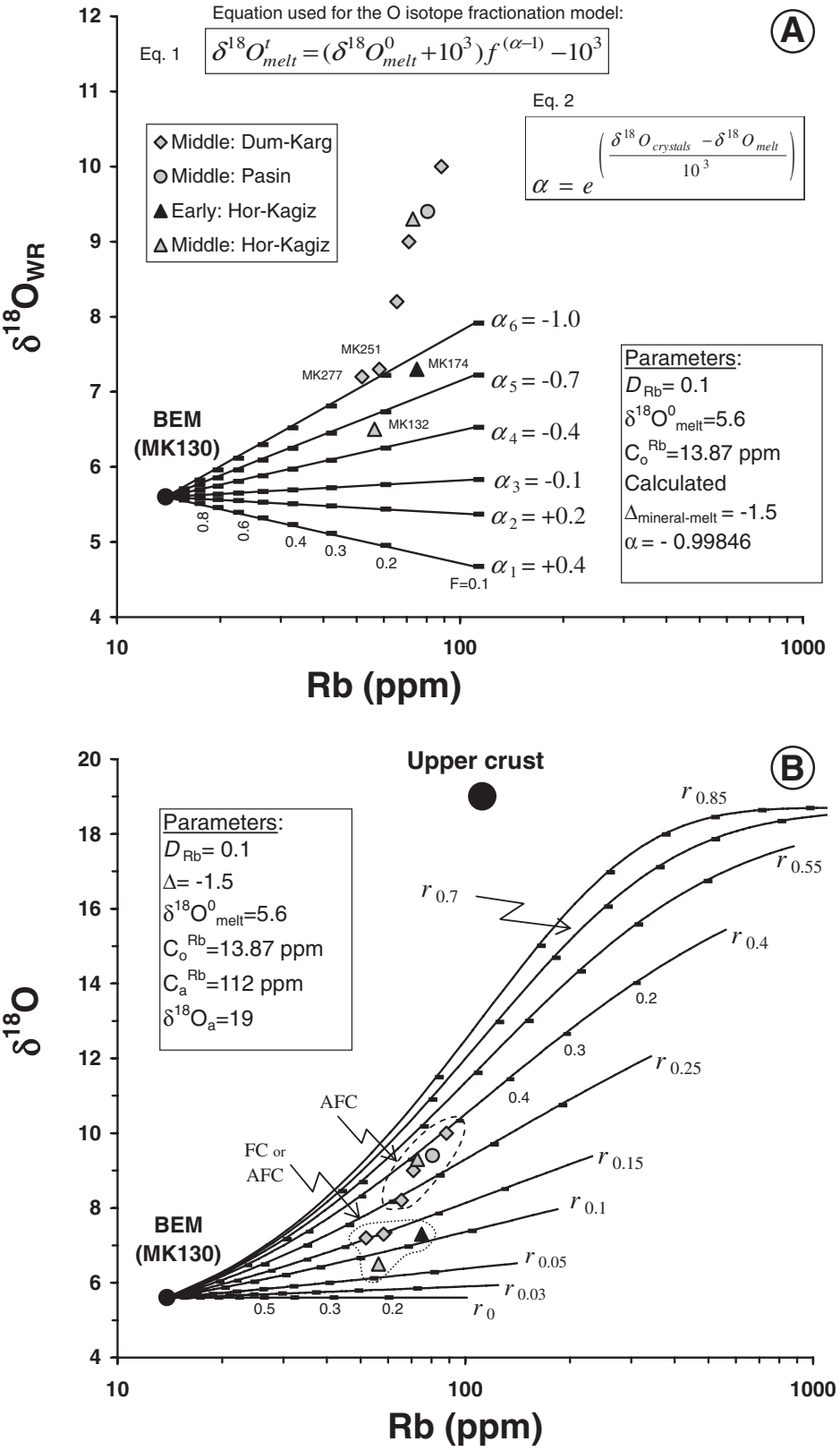

Figure 11. (A) $\delta^{18}O$ versus Rb diagram for nine Erzurum-Kars plateau lavas. The equations given in the insets are taken from Woodhead et al. (1987). The vectors modeled indicate the paths expected from a closed-system fractional crystallization of a parental magma similar in composition to MK130. The symbols are as in Figures 3 and 6. The tic marks on each vector correspond to 10% crystallization intervals. $\delta^{18}O^{0}_{melt}$—the initial O isotope ratio of the melt; $\delta^{18}O^{t}_{melt}$—the $\delta^{18}O$ value of the melt after some specified amount of crystallization; f—the fraction of melt remaining at time "t"; α—the mean solid-magma O isotope fractionation factor. BEM—basaltic end-member. (B) $\delta^{18}O$ versus Rb diagram for Erzurum-Kars plateau lavas displaying the results of assimilation and fractional crystallization (AFC) modeling. FC—the fraction of melt remaining; r—the ratio of the rate of assimilation to the rate of fractional crystallization. The tic marks on each curve represent 5% crystallization intervals. In this model, crystallization ends after FC reaches 0.1. See the text for a thorough discussion.

TABLE 3. REPRESENTATIVE ELECTRON MICROPROBE ANALYSES OF AMPHIBOLE PHENOCRYSTS IN THE LAVAS OF THE ERZURUM-KARS PLATEAU

Mt. Dumlu area: Dumlu formation (porphyritic amphibole dacite/andesite)																
Sample no.	MK36-12b	MK36-14c	MK52A-3d	MK52A-4b	MK90-12a	MK90-12c	MK93-8b	MK93-9a	MK251-1b	MK251-2b	MK251-3a	MK261-1a	MK261-2b	KM228-1c	MK228-2a	MK228-3a
SiO_2	44.18	40.23	45.31	44.92	41.70	42.93	44.15	44.66	42.40	42.37	43.39	42.59	45.44	41.46	43.06	43.43
TiO_2	3.32	3.41	2.88	3.11	2.94	2.97	3.20	3.34	3.87	3.47	3.26	4.02	2.89	3.94	2.82	2.53
Al_2O_3	10.64	10.79	10.30	10.51	11.44	11.50	10.23	10.80	12.56	12.43	11.89	12.01	9.07	12.15	11.67	11.17
Cr_2O_3	.10	.09	.00	.00	.00	.17	.00	.10	.04	.08	.00	.05	.00	.00	.00	.03
FeO	11.70	11.88	12.01	12.08	10.65	11.07	12.12	11.65	13.39	13.37	13.43	13.07	12.28	12.93	14.02	13.70
MnO	0.13	0.16	0.22	0.17	0.26	0.00	0.07	0.00	0.00	0.06	0.27	0.17	0.24	0.22	0.28	0.21
MgO	14.76	14.51	14.69	14.60	13.83	13.69	14.45	14.63	13.28	13.60	13.55	12.92	14.62	13.16	13.54	13.33
CaO	11.57	11.55	11.53	11.47	10.91	10.81	11.51	11.69	11.03	11.34	11.26	11.17	11.89	11.24	11.18	11.24
Na_2O	2.62	2.54	2.29	2.43	2.59	2.52	2.54	2.62	2.60	2.80	2.61	2.55	2.28	2.50	2.46	2.53
K_2O	0.64	0.66	0.61	0.54	0.91	0.86	0.64	0.69	0.72	0.65	0.65	0.78	0.69	0.66	0.64	0.55
NiO	0.00	0.13	0.02	0.22	0.00	0.11	0.00	0.01	0.00	0.00	0.01	0.05	0.00	0.00	0.11	0.00
Total	99.66	99.94	99.86	100.05	95.23	96.64	98.90	100.19	99.88	100.15	100.32	99.38	99.40	98.27	99.78	98.73
Formula																
Si	6.370	6.365	6.502	6.446	6.286	6.363	6.422	6.395	6.140	6.129	6.253	6.197	6.561	6.112	6.260	6.360
Ti	0.360	0.369	0.311	0.336	0.333	0.331	0.350	0.360	0.422	0.377	0.354	0.440	0.314	0.437	0.308	0.279
Al^{TOT}	1.808	1.831	1.742	1.778	2.033	2.009	1.753	1.823	2.143	2.120	2.019	2.060	1.543	2.111	1.999	1.928
Al^{IV}	1.630	1.635	1.498	1.554	1.714	1.637	1.578	1.605	1.860	1.871	1.747	1.803	1.439	1.888	1.740	1.640
Al^{VI}	0.178	0.196	0.244	0.224	0.319	0.372	0.175	0.218	0.283	0.249	0.272	0.257	0.104	0.223	0.259	0.287
Cr	0.011	0.010	0.000	0.000	0.000	0.020	0.000	0.011	0.005	0.009	0.000	0.005	0.000	0.000	0.000	0.004
Fe	1.410	1.430	1.441	1.449	1.343	1.372	1.474	1.396	1.621	1.617	1.619	1.590	1.482	1.593	1.705	1.678
Mn	0.016	0.019	0.027	0.020	0.033	0.000	0.009	0.000	0.000	0.007	0.033	0.021	0.030	0.028	0.035	0.026
Mg	3.173	3.113	3.142	3.123	3.108	3.024	3.133	3.122	2.865	2.933	2.911	2.803	3.146	2.891	2.935	2.911
Ca	1.788	1.781	1.773	1.764	1.763	1.716	1.794	1.794	1.712	1.758	1.739	1.743	1.840	1.775	1.742	1.765
Na	0.732	0.710	0.638	0.675	0.756	0.725	0.716	0.727	0.729	0.785	0.729	0.721	0.638	0.716	0.693	0.719
K	0.117	0.122	0.111	0.100	0.175	0.163	0.118	0.126	0.132	0.119	0.120	0.145	0.126	0.124	0.118	0.103
Ni	0.000	0.015	0.003	0.026	0.000	0.013	0.000	0.002	0.000	0.000	0.001	0.006	0.000	0.000	0.013	0.000
No. of O atoms	23	23	23	23	23	23	23	23	23	23	23	23	23	23	23	23
Total (ions)	15.785	15.765	15.690	15.717	15.830	15.736	15.768	15.755	15.769	15.853	15.777	15.732	15.681	15.787	15.806	15.772

	Pasinler area: Kızılveren formation (porphyritic amphibole dacite/andesite)											Pasinler area: Black ignimbrite				
Sample no.	MK112-10a	MK112-12a	MK112-16b	MK118-1a	MK118-2a	MK118-2c	MK337-1c	MK337-2c	MK337-3a	MK337-4a	MK337-4b	MK106-6b	MK106-6c	MK106-7a	MK106-7b	MK318-2b
SiO_2	44.40	44.38	44.45	45.87	44.04	44.22	45.56	44.41	43.32	43.20	41.97	44.98	45.15	43.34	43.85	43.71
TiO_2	2.70	2.39	2.09	1.90	2.59	2.69	1.33	2.40	2.34	2.73	2.75	3.52	3.70	4.01	4.21	3.95
Al_2O_3	10.85	10.82	10.86	11.61	11.54	11.75	10.35	10.92	10.76	12.76	12.21	10.54	10.47	11.18	11.32	9.73
Cr_2O_3	0.00	0.09	0.17	0.08	0.00	0.00	0.05	0.07	0.02	0.11	0.02	0.00	0.01	0.09	0.09	0.00
FeO	14.57	13.80	14.67	13.85	13.96	13.98	15.01	14.50	15.78	15.19	15.36	10.57	10.66	11.18	11.15	11.95
MnO	0.17	0.33	0.19	0.14	0.25	0.29	0.39	0.34	0.35	0.22	0.27	0.30	0.29	0.32	0.24	0.40
MgO	13.22	13.55	13.06	12.97	12.81	12.90	13.33	13.27	12.14	12.48	11.76	14.69	15.08	13.96	14.38	14.29
CaO	11.23	11.11	11.24	10.62	10.93	10.54	10.10	11.38	10.71	11.13	10.57	11.11	11.04	11.53	11.33	11.29
Na_2O	2.14	2.13	2.16	2.37	2.52	2.60	2.18	2.33	2.10	2.79	2.63	2.65	2.96	2.81	2.91	2.67
K_2O	0.65	0.56	0.64	0.66	0.60	0.61	0.65	0.51	0.64	0.66	0.62	0.80	0.86	0.87	0.79	0.86
NiO	0.00	0.00	0.00	0.00	0.03	0.02	0.00	0.00	0.00	0.00	0.00	0.08	0.00	0.00	0.07	0.20
Total	99.92	99.16	99.54	100.06	99.28	99.58	98.95	100.12	98.16	101.25	98.16	99.24	100.22	99.29	100.32	99.06
Formula																
Si	6.439	6.463	6.475	6.579	6.413	6.411	6.637	6.422	6.430	6.214	6.239	6.468	6.439	6.284	6.279	6.367
Ti	0.295	0.261	0.228	0.205	0.284	0.293	0.145	0.261	0.261	0.295	0.307	0.381	0.396	0.437	0.453	0.433
Al^{TOT}	1.855	1.858	1.864	1.963	1.981	2.008	1.778	1.861	1.883	2.164	2.140	1.787	1.760	1.911	1.910	1.671
Al^{IV}	1.561	1.537	1.525	1.421	1.587	1.589	1.363	1.578	1.570	1.786	1.761	1.532	1.561	1.716	1.721	1.633
Al^{VI}	0.294	0.321	0.339	0.542	0.394	0.419	0.415	0.283	0.313	0.378	0.379	0.255	0.199	0.195	0.189	0.038
Cr	0.000	0.011	0.020	0.009	0.000	0.000	0.005	0.008	0.002	0.013	0.003	0.000	0.001	0.010	0.010	0.000
Fe	1.767	1.680	1.787	1.661	1.700	1.695	1.829	1.754	1.958	1.827	1.910	1.271	1.272	1.356	1.336	1.456
Mn	0.020	0.041	0.024	0.017	0.031	0.035	0.049	0.041	0.044	0.027	0.035	0.036	0.035	0.039	0.029	0.050
Mg	2.857	2.941	2.837	2.774	2.781	2.788	2.896	2.860	2.685	2.676	2.607	3.150	3.206	3.017	3.069	3.102
Ca	1.745	1.733	1.754	1.633	1.706	1.638	1.577	1.764	1.705	1.715	1.683	1.712	1.687	1.790	1.739	1.762
Na	0.601	0.601	0.611	0.658	0.712	0.730	0.616	0.654	0.605	0.777	0.758	0.740	0.818	0.790	0.808	0.755
K	0.120	0.105	0.119	0.120	0.112	0.112	0.120	0.095	0.120	0.121	0.118	0.147	0.157	0.161	0.144	0.161
Ni	0.000	0.000	0.000	0.000	0.003	0.002	0.000	0.000	0.000	0.000	0.000	0.009	0.000	0.000	0.008	0.023
No. of O atoms	23	23	23	23	23	23	23	23	23	23	23	23	23	23	23	23
Total (ions)	15.699	15.695	15.720	15.619	15.724	15.712	15.651	15.719	15.693	15.829	15.799	15.701	15.771	15.794	15.784	15.779

(*continued*)

TABLE 3. *Continued*

	Pasinler area: Black ignimbrite						Pasinler area: Ardıçlıdağ formation (rhyolite)					North of Horasan: Köroğlu formation (porphyritic amphibole Dac/And)	
Sample no.	MK318-3b	MK318-4c	MK318-7a	MK319-2b	MK359-3c	MK359-9a	MK125-2a	MK125-3a	MK125-13b	MK330-9b	MK330-9c	MK133-1a	MK133-2c
SiO_2	43.68	45.94	44.33	45.92	42.58	42.94	43.14	42.84	43.65	42.51	41.74	44.22	43.09
TiO_2	3.96	3.01	3.65	3.17	4.30	3.24	1.99	1.93	1.81	1.83	1.82	1.78	2.61
Al_2O_3	10.28	9.00	10.04	9.30	10.44	10.26	8.12	7.68	7.72	8.08	7.97	12.48	12.39
Cr_2O_3	0.08	0.00	0.20	0.07	0.00	0.00	0.09	0.00	0.00	0.00	0.00	0.19	0.09
FeO	12.27	12.24	11.49	14.10	11.85	12.56	27.27	28.13	28.51	30.72	29.89	12.65	13.06
MnO	0.28	0.36	0.29	0.27	0.34	0.54	1.21	1.55	1.42	1.49	1.86	0.18	0.21
MgO	14.43	15.09	14.75	12.80	13.88	13.88	5.06	3.79	4.19	3.46	3.30	14.06	13.16
CaO	11.38	11.35	11.47	10.46	11.54	11.15	9.95	9.53	9.62	9.67	9.48	10.97	11.17
Na_2O	2.75	2.88	2.61	2.51	2.78	2.94	2.25	2.26	2.46	2.52	2.28	2.52	2.50
K_2O	0.87	0.89	0.66	0.92	0.80	0.79	1.00	1.06	1.11	0.97	1.03	0.50	0.57
NiO	0.05	0.00	0.05	0.00	0.00	0.00	0.17	0.06	0.00	0.00	0.00	0.04	0.00
Total	100.03	100.77	99.53	99.52	98.50	98.30	100.24	98.83	100.47	101.25	99.38	99.59	98.86
Formula													
Si	6.305	6.553	6.388	6.651	6.245	6.326	6.671	6.759	6.767	6.620	6.624	6.371	6.289
Ti	0.429	0.323	0.396	0.346	0.474	0.359	0.232	0.229	0.211	0.214	0.217	0.193	0.287
Al^{TOT}	1.750	1.513	1.706	1.587	1.806	1.781	1.480	1.428	1.411	1.484	1.490	2.119	2.131
Al^{IV}	1.695	1.447	1.612	1.349	1.755	1.674	1.329	1.241	1.233	1.380	1.376	1.629	1.711
Al^{VI}	0.055	0.066	0.094	0.238	0.051	0.107	0.151	0.187	0.178	0.105	0.115	0.490	0.420
Cr	0.009	0.000	0.023	0.008	0.000	0.000	0.011	0.000	0.000	0.000	0.000	0.022	0.011
Fe	1.481	1.460	1.384	1.708	1.453	1.548	3.526	3.712	3.696	4.002	3.968	1.524	1.594
Mn	0.034	0.044	0.035	0.033	0.042	0.068	0.158	0.208	0.186	0.196	0.250	0.022	0.026
Mg	3.105	3.209	3.169	2.762	3.035	3.048	1.167	0.892	0.969	0.804	0.782	3.020	2.863
Ca	1.761	1.735	1.772	1.624	1.813	1.761	1.649	1.611	1.598	1.614	1.613	1.694	1.747
Na	0.770	0.797	0.730	0.705	0.790	0.840	0.674	0.692	0.738	0.760	0.702	0.704	0.708
K	0.161	0.162	0.121	0.170	0.150	0.147	0.196	0.212	0.219	0.192	0.208	0.092	0.106
Ni	0.005	0.000	0.005	0.000	0.000	0.000	0.021	0.008	0.000	0.000	0.000	0.005	0.000
No. of O atoms	23	23	23	23	23	23	23	23	23	23	23	23	23
Total (ions)	15.810	15.795	15.730	15.594	15.808	15.878	15.786	15.751	15.795	15.886	15.854	15.764	15.761

	North of Horasan: Köroğlu formation (porphyritic amphibole Dac/And) (*cont.*)				S of Horasan: Saçdağ fm.		N of Horasan: Horasan fm. (plateau)		Kağızman area: Paslı formation (Tr-Dac)			
Sample no.	MK140-1a	MK140-2b	MK140-3a	MK140-4b	MK154-5e	MK154-6b	MK134-5a	MK134-11b	MK174-1a	MK174-2d	MK174-3C1	MK174-3R1
SiO_2	45.60	45.42	44.57	44.75	43.46	45.27	45.28	45.31	41.36	41.86	42.16	40.48
TiO_2	2.25	2.28	2.13	2.34	2.27	1.21	2.47	2.60	3.65	3.31	3.44	2.97
Al_2O_3	10.58	10.10	10.93	10.35	12.87	11.40	10.01	9.66	12.44	11.76	11.25	10.83
Cr_2O_3	0.04	0.20	0.00	0.15	0.05	0.07	0.17	0.10	0.00	0.00	0.00	0.04
FeO	13.69	13.70	12.96	13.39	14.07	15.17	12.25	11.96	17.76	16.94	16.80	16.21
MnO	0.13	0.26	0.13	0.32	0.27	0.27	0.18	0.12	0.31	0.58	0.47	0.45
MgO	13.13	14.02	14.28	13.58	12.67	12.93	14.96	15.27	10.92	11.07	11.80	11.21
CaO	11.22	11.49	11.44	11.34	11.19	10.99	11.57	11.46	10.70	10.54	10.95	12.74
Na_2O	2.40	1.93	2.24	2.36	2.50	2.25	2.47	2.27	2.85	2.59	2.72	2.39
K_2O	0.62	0.47	0.41	0.54	0.63	0.51	0.39	0.53	0.65	0.63	0.57	0.61
NiO	0.14	0.00	0.07	0.04	0.00	0.00	0.11	0.10	0.03	0.00	0.00	0.00
Total	99.80	99.86	99.18	99.16	99.97	100.08	99.84	99.35	100.67	99.29	100.15	97.93
Formula												
Si	6.568	6.540	6.449	6.500	6.293	6.546	6.509	6.535	6.085	6.211	6.203	6.134
Ti	0.243	0.247	0.232	0.256	0.247	0.132	0.267	0.282	0.404	0.370	0.380	0.338
Al^{TOT}	1.798	1.713	1.865	1.773	2.197	1.942	1.697	1.642	2.156	2.057	1.951	1.934
Al^{IV}	1.432	1.460	1.551	1.500	1.707	1.454	1.491	1.465	1.915	1.789	1.797	1.866
Al^{VI}	0.365	0.253	0.313	0.273	0.490	0.488	0.206	0.177	0.241	0.268	0.154	0.068
Cr	0.004	0.022	0.000	0.017	0.006	0.008	0.019	0.012	0.000	0.000	0.000	0.005
Fe	1.651	1.650	1.568	1.627	1.704	1.835	1.472	1.443	2.186	2.102	2.068	2.054
Mn	0.016	0.031	0.016	0.039	0.032	0.033	0.022	0.015	0.038	0.073	0.058	0.058
Mg	2.821	3.009	3.081	2.942	2.735	2.787	3.205	3.282	2.393	2.448	2.588	2.532
Ca	1.732	1.773	1.774	1.766	1.736	1.702	1.782	1.771	1.687	1.676	1.727	2.068
Na	0.669	0.539	0.629	0.664	0.702	0.632	0.688	0.634	0.814	0.745	0.776	0.702
K	0.114	0.087	0.076	0.101	0.117	0.094	0.072	0.097	0.122	0.119	0.107	0.118
Ni	0.016	0.000	0.008	0.004	0.000	0.000	0.012	0.011	0.004	0.000	0.000	0.000
No. of O atoms	23	23	23	23	23	23	23	23	23	23	23	23
Total (ions)	15.631	15.610	15.697	15.688	15.768	15.710	15.746	15.722	15.889	15.802	15.858	15.943

Notes: See text for details.

tallization) by utilizing this type of modeling. Figure 11B shows that, except for the samples with $\delta^{18}O$ contents that might have been controlled by isotope fractionation (the ones with $\delta^{18}O$ values lower than +7.5‰), intermediate lavas of the middle stage display a significant crustal assimilation, with *r* values clustering between 0.2 and 0.4. These results are consistent with the results of trace-element AFC modeling conducted on the samples from the same area (see Fig. 7B *in* Keskin et al., 1998).

Crystallization Pressures as a Measure of the Depth of Equilibration

The linear increase in the Al^{TOT} content of magmatic amphibole with pressure can be utilized as a tool to calculate the depth of the magma chambers in which the crystallization of amphibole took place. The utility of Al in magmatic hornblende as a geobarometer has been developed in a number of papers (e.g., Hammarstrom and Zen, 1986; Hollister et al., 1987; Johnson and Rutherford, 1989; Schmidt, 1992). Among others, the Johnson and Rutherford (1989) calibration is a better choice for calculating the crystallization pressures of the amphiboles in the lavas of the Erzurum-Kars plateau, because the calibration was made for magmas fractionating at more appropriate temperatures.

In this study, we calculated solidus pressures for 57 amphibole phenocrysts (Table 3) by applying Johnson and Rutherford's (1989) equation. We calculated the equilibrium depths of the amphiboles by using these results and assuming an average density for the crust of 2700 kg/m^{-3}. Note that the error arising from the uncertainty of Johnson and Rutherford's (1989) calibration is ± 0.5 kb. This corresponds to a depth range of ±1.9 km as displayed in Figure 12.

Figure 12 shows that the lavas of the middle stage dominantly plot into a depth range of between ~15 and 22 km, whereas those of the early stage fall into a range of 18–22 km (the Paslı formation in the Kağızman area; Fig. 12). Given that the crustal thickness in Eastern Anatolia is ~40 km (Zor et al., 2003), the amphiboles must have crystallized in the midcrust (in a three-layer crustal model) or the lower crust (in a two-layer model). In contrast, the volcanic units of the late stage require crystallization

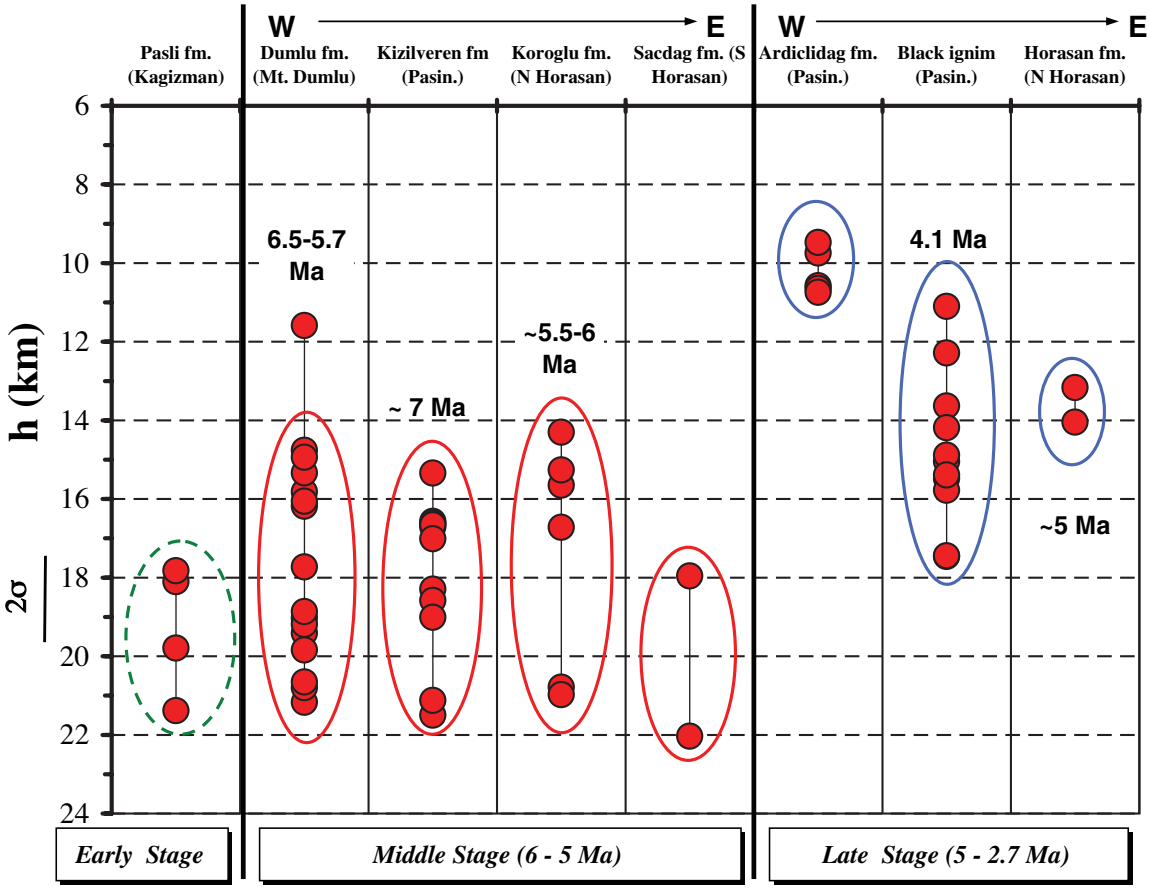

Figure 12. Crystallization depths calculated from crystallization pressures of the amphibole phenocrysts enclosed in the lavas of the Erzurum-Kars plateau. Johnson and Rutherford's (1989) Al-in-hornblende geobarometer equation has been used in the calculation of crystallization pressures. For details, see the text.

at relatively shallow depths of between ~10 and 16 km. This implies that lavas of the late stage evolved, in part, at upper-crustal depths. Note that some lavas contain both high- and low-pressure crystals (e.g., MK228, MK251, and MK337). The coexistence of such phenocrysts may be ascribed to at least two phases of amphibole crystallization at different depths. This supports the views presented in previous studies of Pearce et al. (1990) and Keskin et al. (1998) that fractionation may be polybaric.

Composition and Nature of the Assimilants: Crustal Domains beneath the Erzurum-Kars plateau

On Pb-Pb isotope covariation diagrams (Fig. 7), lavas from the western part of the Erzurum-Kars plateau (i.e., Mount Dumlu and Kargapazarı areas) and those from the eastern part of the plateau (i.e., the Horasan, Aladağ, and Kağızman areas) form two separate trends, starting from a common primitive magma composition (i.e., MK130) and diverging toward two contrasting end-member compositions. Because samples do not follow the source contamination curve on a $^{208}Pb/^{204}Pb_{(i)}$ versus $\delta^{18}O$ plot (Fig. 10F), we argue that contamination of the mantle source by subduction cannot account for this relationship. Because this Pb isotopic ratio correlates significantly with both SiO_2 and $\delta^{18}O$, and AFC models indicate that assimilation was an important process in magma evolution beneath the Erzurum-Kars plateau (Fig. 11), these end-member compositions correspond to two different and isotopically distinct crustal compositions beneath the plateau. If that is the case, variations on Pb-Pb isotopic plots might be controlled by the composition and the amount of crustal material assimilated by the magmas. These results raise questions over whether these compositional differences are a reflection of the presence of two different crustal domains beneath the western and eastern parts of the Erzurum-Kars plateau or the internal stratification of the crust.

The radiogenic crustal end-member, which is supposed to have been assimilated by the lavas of the eastern part of the Erzurum-Kars plateau, is broadly similar in its Pb isotopic composition to the upper crust, while the unradiogenic one, which is presumed to have been assimilated by the lavas of the western part of the plateau, plots into a field commonly occupied by lower-crustal rocks (Fig. 7). Magma chambers residing deeper (i.e., ~22–15 km; Fig. 3) beneath the western part of the plateau might have resided in the lower crust, assimilating unradiogenic material, in contrast to those beneath the eastern part of the plateau, which emplaced in the upper crust, assimilating upper-crustal material. However, such a model fails to explain why the lavas derived from deeper chambers in the eastern part of the plateau (i.e., the Pasli formation in the Kağızman area, ~16–22 km; Fig. 12) still have radiogenic Pb. Therefore, it is likely that the geochemical data are more compatible with a model involving interactions between a common primitive magma and two different crustal domains beneath the eastern and the western parts of the Erzurum-Kars plateau.

As pointed out earlier in the section on geology, the volcanic units of the studied part of the Erzurum-Kars plateau are assumed to overlie two different tectonic blocks: (1) the Rhodope-Pontide basement and (2) the Northwest Iranian fragment (Fig. 1). Because volcanic units of the plateau mask the basement units over great distances, the lateral extent and location of these crustal domains beneath the plateau are not known. The geological map presented by Şengör et al. (2003) indicates that the western part of the plateau overlies the Rhodope-Pontide fragment, while the volcanic units of the eastern part probably overlie the Northwest Iranian fragment (Fig. 1). On the basis of these results and interpretations, it can be argued that unradiogenic material assimilated by the volcanic units of the western part of the plateau possibly corresponds to the continental crust of the Rhodope-Pontide fragment (i.e., CT-1 in Fig. 7), whereas radiogenic material assimilated by the volcanic products on the eastern part of the plateau (i.e., CT-2 in Fig. 7) coincides with the continental crust of the Northwest Iranian fragment. Because the volcanic units from the Pasinler area display transitional isotopic characteristics between the western and eastern parts of the plateau, this area may be located on the inferred tectonic border between these two continental blocks. The Rhodope-Pontide basement may owe most of its isotopic signature to the long-lasting arc-related volcanic activity between the Cretaceous and the early Eocene. Assimilation of such material by mantle-derived magmas can likely generate trends similar to those shown by the lavas from the western part of the plateau on the isotope covariation diagrams.

Evolution of the Magma Plumbing System beneath the Erzurum-Kars Plateau

The model we propose for spatial and temporal evolution of the magma plumbing system beneath the Erzurum-Kars plateau is illustrated via a series of west-east lithospheric cross-sections in Figure 13, corresponding to various stages of the volcanism. As can be seen in Figure 13, the Rhodope-Pontide fragment possibly underlies the western part of the plateau (i.e., Mount Dumlu and Kargapazarı areas), whereas the Northwest Iranian fragment underlies the eastern part of the plateau beneath the Horasan, Aladağ, and Kağızman areas (see Fig. 1). The phase diagram of Foden and Green (1992) is presented beside the figures to explain the variations in crystallization assemblages with depth. The overall setting beneath the Erzurum-Kars plateau is probably more compatible with a model that involves the delamination of tectonically thickened mantle lithosphere. It is beyond the scope of this article to discuss the geodynamic models proposed in previous studies for the tectonomagmatic evolution of eastern Anatolia; general reviews of these have been presented by Pearce et al. (1990), Keskin et al. (1998), and Keskin (2003, 2005, forthcoming).

The volcanostratigraphic and geochemical data indicate that the first collision-related lavas on the Erzurum-Kars plateau, mainly anhydrous calc-alkaline basalts, were erupted at ca. 11 Ma in the Horasan area (Fig. 13A; see also the Kotek

basalt, Fig. 2). This was followed by volcanism in the Pasinler area (i.e., the Black dacite in Fig. 2) ca. 8 Ma (Fig. 13A). Note that the volcanism was quite sporadic, while the assimilation of the crustal material was very limited during this stage.

Between 7 and 6 Ma, bimodal anhydrous lavas and pyroclastic units erupted on the western and central parts of the plateau (i.e., the Dumlu, Kargapazarı, and Horasan areas; Fig. 13B). Trace-element AFC models (Keskin et al., 1998) indicate that crystallization was dominated by anhydrous phases with minor assimilation of upper crust, or none, throughout the early stage. The volcanic material produced during this stage deposited in and around the pull-apart basins (in the Karasu and Pasinler basins in the north of Erzurum and in the Horasan basin) controlled by strike-slip fault systems (e.g., the Erzurum-Tbilisi fault zone) (Keskin et al., 1998). Intermediate to acid lavas and pyroclastic products were derived from large, shallow (~16–9 km), compositionally zoned magma chambers. The evolution of magma via FC associated by degassing in these large, shallow magma chambers possibly triggered pyroclastic explosive eruptions on the plateau (Fig. 13B). Basic lavas, on the other hand, were possibly drained either from small, shallow, transient chambers or directly from the source region through deep fractures (Keskin et al., 1998). These deep fractures, possibly associated with strike-slip fault systems, tapped the most primitive lavas of this stage. Amphibole did not crystallize in these chambers, because they were likely shallower than 10–13 km (i.e., see the phase diagram of Foden and Green, 1992, in Fig. 13).

During the middle stage (i.e., 6–5 Ma), volcanic activity was more intensive in the western part of the Erzurum-Kars plateau (Fig. 13C). Magmas ponded and homogenized in large, compositionally or thermally zoned chambers that fed crystal-rich, isolated intermediate domes on the plateau. Al in amphibole geobarometry results (Fig. 12) indicate that the magma chambers were located deeper (14–22 km) beneath the plateau than those of the late stage (Fig. 13C). The results of AFC models based on trace elements (Fig. 7B *in* Keskin et al., 1998) and $\delta^{18}O$ (Fig. 11B) indicate that crystallization of Plg + Amp–dominated phases was accompanied by the assimilation of a significant amount of crustal material, which was possibly represented by the lower crust. Widespread amphibole fractionation resulted in the formation of the low-Y lava series (Y < 20 ppm; Keskin et al., 1998). We argue that both the emplacement of magma chambers at greater crustal depths and the presence of greater crustal assimilation can be linked to the domination of a compressional regime in the region during this period, possibly due to a major modification in the lithospheric stress field. As proposed by Örgülü et al. (2003) and Koçyiğit et al. (2001), the crustal stress field has changed dramatically during the past 5–10 m.y. However, further research on temporal and spatial change of the stress field in the region is needed in order to better understand the underlying reason.

The ratio of lavas to pyroclastic material greatly increased during the late stage between 5 and 1.5 Ma, and their composition became more basic compared to the lavas of the early and middle stages (Fig. 13D and E). Petrographic data indicate that magmas crystallized anhydrous phases during the late stage. The AFC modeling based on trace-element behavior (Keskin et al., 1998) implies that the assimilation of the crustal material was limited. This indicates that magmas either evolved in very small and shallow chambers or rose directly to the surface. However, variations in isotopic ratios (especially those of Pb) still show some degree of assimilation of crustal material in these chambers. Temporal variations during the late stage may be linked to the increasing effects of extensional structures related to the strike-slip fault systems that resulted in the formation of networks of fractures through which magmas were injected (Fig. 13E). This must be the reason that magmas were better drained to the surface without significantly interacting with the crust, forming extensive basaltic lava fields on the Erzurum-Kars plateau during the late stage, especially in the eastern part of the plateau (i.e., the Horasan, Aladağ, and Kağızman areas). Volcanism migrated to the east on the plateau, while subaerial clastic beds were deposited coeval with the volcanic units. The most primitive lavas erupted in the eastern part of the Erzurum-Kars plateau close to the end of this period.

CONCLUSIONS

The geochemical evidence presented in this study indicates that the mantle source varied little with time. However, although the primitive magma composition is almost constant, the petrography and trace-element chemistry of the volcanic products provide evidence for a systematic temporal variation of the volcanic activity throughout the Erzurum-Kars plateau. It began with the eruption of anhydrous bimodal volcanic products during the early stage (i.e., 11–6 Ma), then changed abruptly into a unimodal volcanism dominated by the hydrous lavas of intermediate composition in the middle stage (i.e., 6–5 Ma), and finally returned to the bimodal activity that produced anhydrous lavas during the late stage (i.e., 5–2.7 Ma). These variations were strongly dependent upon the depth of the magma chambers from which the volcanic products were derived. The magma chambers of the middle stage formed deeper (~22–15 km) in the crust in comparison with those of the early and late stages, possibly in response to the dominantly compressional regime of this period. Magmas in these deeper chambers fractionated amphi-

Figure 13 (*on following three pages*). The magma plumbing model proposed for the collision-related volcanism on the Erzurum-Kars plateau illustrated on crustal sections. Note that the vertical scale for the volcanic sequence is exaggerated in order to show details. Solidified magma chambers are marked by darker colors (circular gradual fill from gray to black). This work constrains the model by placing constraints on the depth of magma chambers, the extent of crust-magma interaction, and the composition of the assimilated crust in space and time. For details, see the text. CT1—crust type 1; CT2—crust type 2; LC—lower crust; L+V—liquid and volatiles; UC—upper crust.

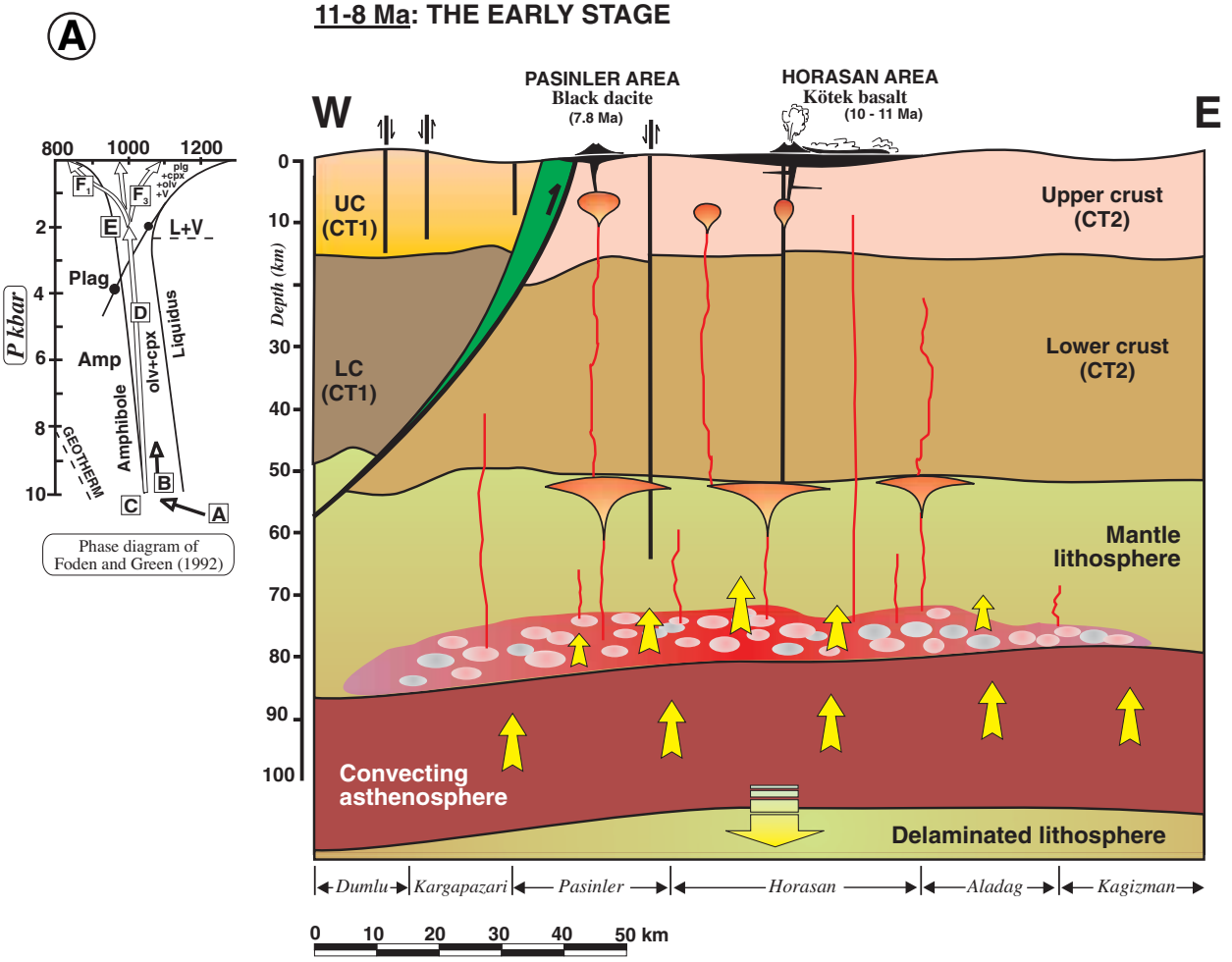

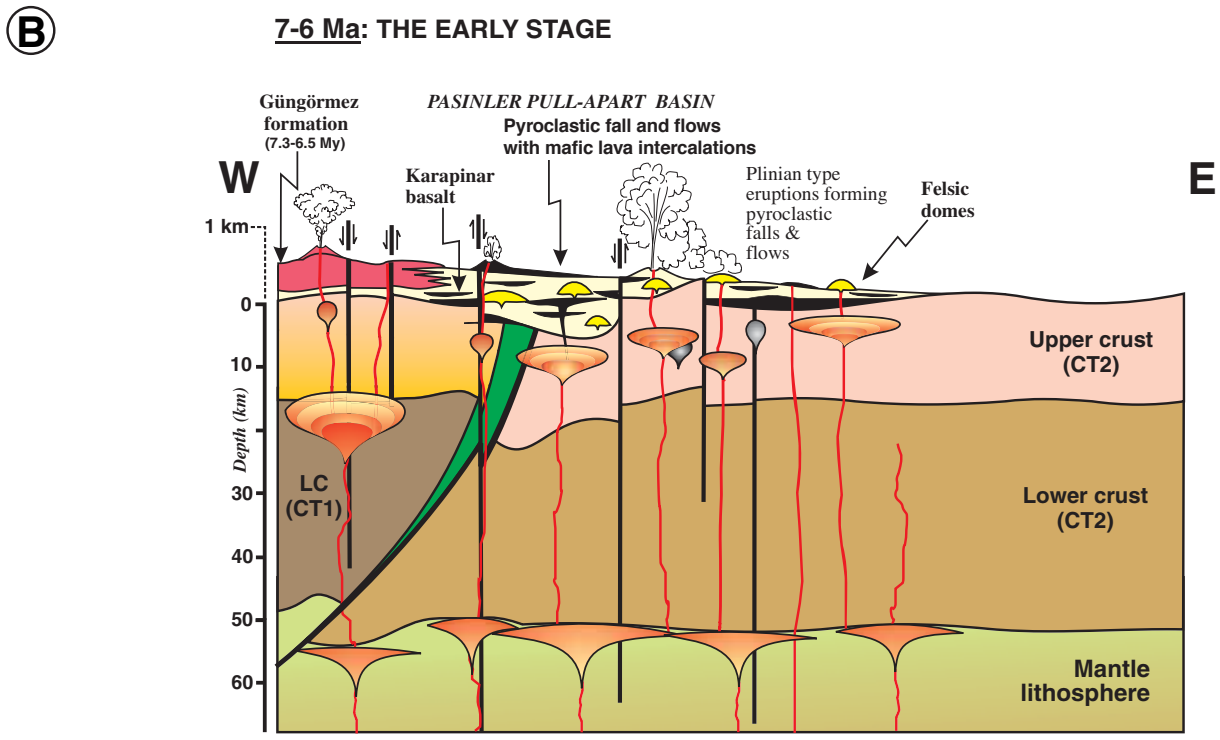

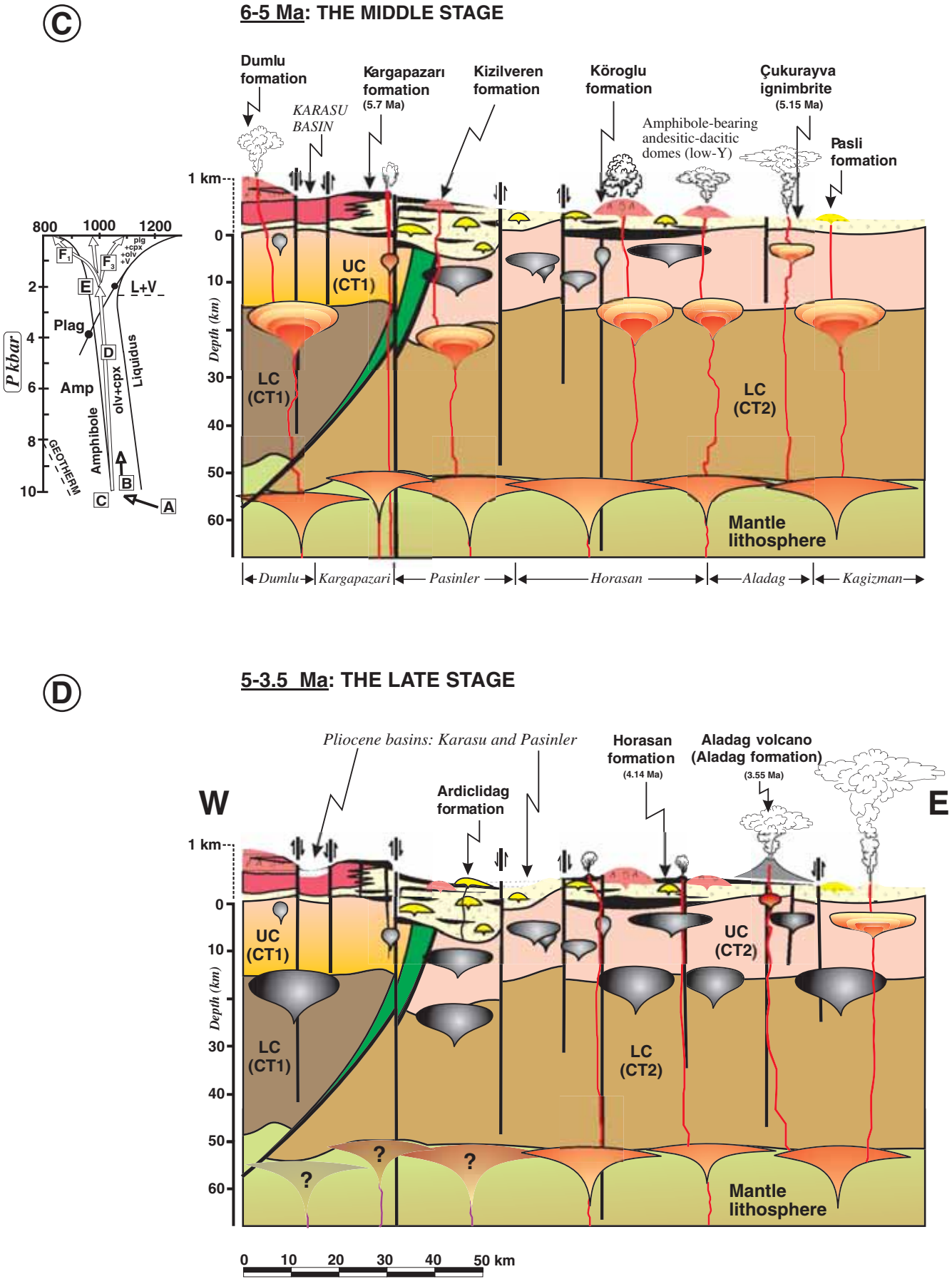

Figure 13. *Continued*

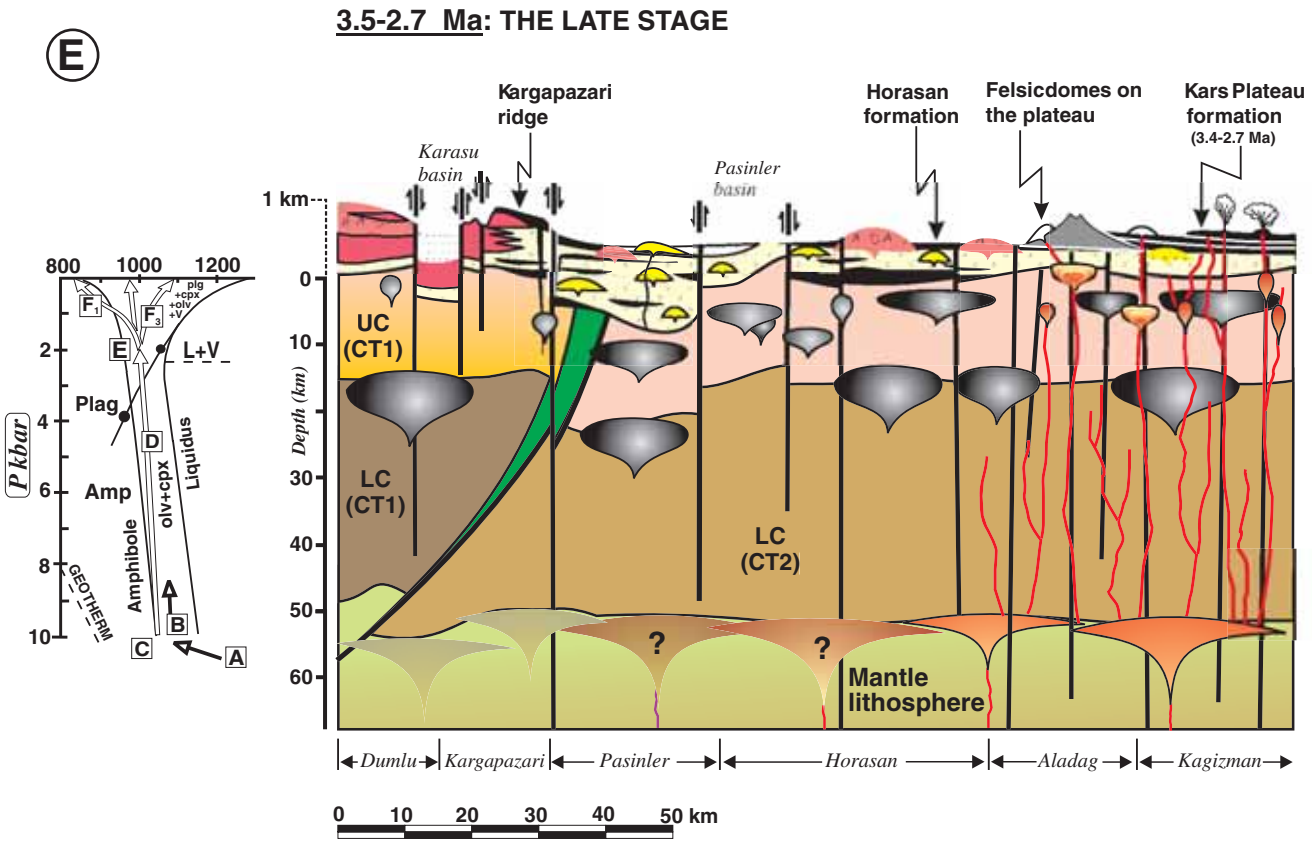

Figure 13. *Continued*

bole, assimilated a significant amount of crustal material, and homogenized by replenishment. In contrast, magmas emplaced in the shallower chambers (~15–9 km) during the early and late stages crystallized anhydrous phases with no amphibole.

In contrast to the behavior of trace elements, the isotopic compositions of the volcanic units do not show a systematic temporal variation in any given subarea on the Erzurum-Kars plateau; instead they exhibit spatial changes. These variations are best reflected by Pb isotopes. Lavas from the eastern part of the plateau (i.e., the Horasan, Aladağ, and Kağızman areas) are much more radiogenic than those from the western part (i.e., the Dumlu and Kargapazarı areas) in terms of their Pb isotopic ratios, and lavas from the Pasinler area display transitional isotopic characteristics between these two groups (Fig. 7). Our isotopic data indicate that these variations may be related to the composition and the amount of crustal material assimilated by the magmas beneath the Erzurum-Kars plateau. We thus argue that two isotopically distinct crustal domains, underlain and hence masked by thick volcanic successions of the plateau, exist beneath the plateau: (1) a more radiogenic crustal domain represented by the Northwest Iranian fragment in the east and (2) the Rhodope-Pontide fragment in the west. Unfortunately, the trace-element and isotopic compositions of the Rhodope-Pontide and the Northwest Iranian crustal domains are almost completely unknown except for some trace-element data from the Pulur complex in the Pontides (Topuz et al., 2004) in the north and $^{87}Sr/^{86}Sr$ isotope data from the Tsakhkuniats basement outcrop in Armenia (Karapetian et al., 2001), located far away from the area studied. Both the Rhodope-Pontide and the Northwest Iranian basements are quite heterogeneous in terms of the lithologies they contain as well as their geochemical compositions. Therefore, it is rather difficult to constrain the crustal compositions of the Rhodope-Pontide and the Northwest Iranian fragments by the data presented in the literature, and further research is needed for isotopic characterization of these two blocks beneath the Erzurum-Kars plateau.

From a global perspective, this work emphasizes the importance of thickened crust in modifying the composition and mineralogy of postcollision volcanic rocks. The ponding of magmas beneath the brittle upper crust, evident here in the middle stages of volcanic evolution, can produce relatively homogeneous intermediate magmas and probably large, zoned batholith-like intrusions at depth. In contrast, smaller chambers ponding within the upper crust, evident here in the early and late

stages of evolution, are more likely to produce bimodal volcanic products and smaller, more localized plutons. In both cases, the regional geochemical variations emphasize the fact that the isotopic signatures of the volcanic eruptions may be significantly influenced by the nature and history of the crustal domains invaded by the magma. The Erzurum-Kars plateau is one of the few collision zones where the volcanic history can be documented in a tectonic context, and it will be interesting to discover whether similar features can be identified in less well-exposed or more deeply eroded collision terranes elsewhere.

ACKNOWLEDGMENTS

We are grateful to the Turkish Ministry of Education for providing Mehmet Keskin with a generous grant. We also thank the Natural Environment Research Council, Isotope Geosciences Laboratories at Nottingham, for allowing us to use their excellent analytical facility. We are grateful to the geologists of the Exploration Division of the Turkish Petroleum Company (TPAO), who provided support during our field work on the Erzurum-Kars plateau. We thank geologists from the Mineral Research and Exploration Institute of Turkey (MTA) for making their field camp facilities available during our field work. We thank Dr. Andrew Peckett for assistance with microprobe work. Special thanks to Dr. Judy Monthie-Doyum and Dr. Belma Haznedar for proofreading an earlier version of the text. The manuscript has been greatly improved by the reviews of Lang Farmer and Kent C. Condie and by comments from Yildirim Dilek.

We thank Professor Gillian R. Foulger for her constant understanding and encouragement, which had a great impact during the writing of this paper. Thanks also go to staff members of the Department of Earth Sciences, University of Durham, England, for kindly making their research facilities available to Mehmet Keskin during his sabbatical leave and for providing him with a stimulating research environment.

REFERENCES CITED

Alıcı, P., Temel, A., and Gaurgaud, A., 2002, Pb-Nd-Sr isotope and trace element geochemistry of Quaternary extension-related alkaline volcanism: A case study of Kula region (Western Anatolia, Turkey): Journal of Volcanology and Geothermal Research, v. 115, p. 487–510.

Bottinga, Y., and Javoy, M., 1975, Oxygen isotope partitioning among the minerals in igneous and metamorphic rocks: Reviews of Geophysics, v. 13, p. 401–418.

Deniel, C., Aydar, E., and Gourgaud, A., 1998, The Hasan Dagi stratovolcano (Central Anatolia, Turkey): Evolution from calc-alkaline to alkaline magmatism in a collision zone: Journal of Volcanology and Geothermal Research, v. 87, p. 275–302, doi: 10.1016/S0377-0273(98)00097-3.

De Paolo, D.J., 1981, Trace element and isotopic effects of combined wall-rock assimilation and fractional crystallisation: Earth and Planetary Science Letters, v. 53, p. 189–202, doi: 10.1016/0012-821X(81)90153-9.

Dewey, J.F., Hempton, M.R., Kidd, W.S.F., Şaroğlu, F., and Şengör, A.M.C., 1986, Shortening of continental lithosphere: The neotectonics of eastern Anatolia, a young collision zone, *in* Coward, M.P., and Ries, A.C., eds., Collision tectonics Geological Society of London Special Publication 19, p. 3–36.

Foden, J.D., and Green, D.H., 1992, Possible role of amphibole in the origin of andesite: Some experimental and natural evidence: Contributions to Mineralogy and Petrology, v. 109, p. 479–493, doi: 10.1007/BF00306551.

Hammarstrom, J.M., and Zen, E-an, 1986, Aluminum in hornblende: An empirical igneous geobarometer: American Mineralogist, v. 71, p. 1297–1313.

Harmon, R.S., Thorpe, R.S., and Francis, P.W., 1981, Petrogenesis of Andean andesites from combined O-Sr isotope relationships: Nature, v. 290, no. 5805, p. 396–399, doi: 10.1038/290396a0.

Hart, S.R., 1984, A large scale isotope anomaly in the Southern Hemisphere mantle: Science, v. 309, p. 753–757.

Hollister, L.S., Grissom, G.C., Peters, E.K., Stowell, H.H., and Sisson, V.B., 1987, Confirmation of empirical correlation of Al in hornblende with pressure of solidification of calc-alkaline plutons: American Mineralogist, v. 72, p. 231–239.

Irvine, T.N., and Baragar, W.R.A., 1971, A guide to the chemical classification of the common volcanic rocks: Canadian Journal of Earth Sciences, v. 8, p. 523–548.

Javoy, M., Fourcade, S., and Allegre, C.J., 1970, Graphical method for examining $^{18}O/^{16}O$ fractionation in silicate rocks: Earth and Planetary Science Letters, v. 10, p. 12–16, doi: 10.1016/0012-821X(70)90059-2.

Johnson, M.C., and Rutherford, M.J., 1989, Experimental calibration of the aluminum-in-hornblende geobarometer with application to Long Valley caldera (California) volcanic rocks: Geology, v. 17, p. 837–841, doi: 10.1130/0091-7613(1989)017<0837:ECOTAI>2.3.CO;2.

Karapetian, S.G., Jrbashian, R.T., and Mnatsakanian, A.K., 2001, Late collision rhyolitic volcanism in the north-eastern part of the Armenian Highland: Journal of Volcanology and Geothermal Research, v. 112, nos. 1–4, p. 189–220, doi: 10.1016/S0377-0273(01)00241-4.

Keskin, M., 2003, Magma generation by slab steepening and breakoff beneath a subduction-accretion complex: An alternative model for collision-related volcanism in Eastern Anatolia, Turkey: Geophysical Research Letters, v. 30, no. 24, p. 8046, doi:10.1029/ 2003GL018019.

Keskin, M., 2005, Domal uplift and volcanism in a collision zone without a mantle plume: Evidence from Eastern Anatolia: http://www.mantleplumes.org/Anatolia.html.

Keskin, M., forthcoming, Eastern Anatolia: A hot spot in a collision zone without a mantle plume, *in* Foulger, G.R., and Jurdy, D., eds., The origins of melting anomalies: Plumes, plates, and planetary processes (P^4 book): Geological Society of America Special Publication.

Keskin, M., Pearce, J.A., and Mitchell, J.G., 1998, Volcano-stratigraphy and geochemistry of collision-related volcanism on the Erzurum-Kars Plateau, North Eastern Turkey: Journal of Volcanology and Geothermal Research, v. 85, nos. 1–4, p. 355–404, doi: 10.1016/S0377-0273(98)00063-8.

Koçyiğit, A., Yılmaz, A., Adamia, S., and Kuloshvili, S., 2001, Neotectonics of East Anatolian Plateau (Turkey) and Lesser Caucasus: Implication for transition from thrusting to strike-slip faulting, Geodinamica Acta, v. 14, nos. 1– 3, p. 177–195.

Kuno, H., 1966, Lateral variation of basalt magma types across continental margins and island arcs: Bulletin of Volcanology, v. 29, p. 195–222.

Kyser, T.K., 1986, Stable isotope variations in the mantle, *in* Valley, J.W., et al., eds., Stable isotopes in high temperature geological processes: Reviews in Mineralogy, vol. 16: Mineralogical Society of America, Washington, D.C, p. 141–164.

Le Bas, M.J., Le Maitre, R.W., Streckeisen, A., and Zanettin, B., 1986, A chemical classification of volcanic rocks based on the total alkali–silica diagram: Journal of Petrology, v. 27, p. 745–750.

Lustrino, M., and Dallai, L., 2003, On the origin of EM-I end-member: Neues Jahrbuch für Mineralogie–Abhandlungen, v. 179, no. 1, p. 85–100.

Notsu, K., Fujitani, T.Ui., Matsuda, J., and Ercan, T., 1995, Geochemical features of collision-related volcanic rocks in central and eastern Anatolia, Turkey: Journal of Volcanology and Geothermal Research, v. 64, p. 171–192.

Örgülü, G., Aktar, M., Türkelli, N., Sandvol, E., and Barazangi, M., 2003, Contribution to the seismotectonics of the Eastern Anatolian Plateau from moderate and small size events: Geophysical Research Letters, v. 30, no. 24, art. no. 8040, doi: 10.1029/2003GL018258.

Pearce, J.A., 1983, Role of the sub-continental lithosphere in magma genesis at active continental margins, *in* Hawkesworth, C.J., and Norry, M.J., eds., Continental basalts and mantle xenolites: Nantwich, Shiva, p. 230–249.

Pearce, J.A., Bender, J.F., De Long, S.E., Kidd, W.S.F., Low, P.J., Guner, Y., Şaroğlu, F., Yılmaz, Y., Moorbath, S., and Mitchell, J.G., 1990, Genesis of collision volcanism in Eastern Anatolia, Turkey: Journal of Volcanology and Geothermal Research, v. 44, p. 189–229, doi: 10.1016/0377-0273(90)90018-B.

Peccerillo, A., and Taylor, S.R., 1976, Geochemistry of Eocene calc-alkaline volcanic rocks from the Kastamonu area, northern Turkey: Contributions to Mineralogy and Petrology, v. 58, p. 63–81, doi: 10.1007/BF00384745.

Rollinson, H.R., 1993, Using geochemical data: Evaluation, presentation, interpretation: New York, Longman, 252 p.

Schmidt, W.S., 1992, Amphibole composition in tonalite as a function of pressure: An experimental calibration of the Al-in-hornblende barometer: Contributions to Mineralogy and Petrology, v. 110, p. 304–310, doi: 10.1007/BF00310745.

Şengör, A.M.C., 1990, A new model for the late Palaeozoic–Mesozoic tectonic evolution of Iran and implications for Oman, *in* Robertson, A.H.F., et al., eds., The geology and tectonics of the Oman region: Geological Society of London Special Publication 49, p. 797–831.

Şengör, A.M.C., and Kidd, W.S.F., 1979, Post-collisional tectonics of the Turkish-Iranian plateau and a comparison with Tibet: Tectonophysics, v. 55, p. 361–376, doi: 10.1016/0040-1951(79)90184-7.

Şengör, A.M.C., Ozeren, S., Genç, T., and Zor, E., 2003, East Anatolian high plateau as a mantle-supported, northsouth shortened domal structure: Geophysical Research Letters, v. 30, no. 24, p. 8045, doi: 10.1029/2003GL017858.

Sun, S.S., and McDonough, W.F., 1989, Chemical and isotopic systematics of oceanic basalts: Implications for mantle composition and processes, *in* Saunders, A.D., and Norry, M.J., eds., Magmatism in ocean basins: Geological Society of London Special Publication 42, p. 313–345.

Taylor, H.P., Jr., 1968, The oxygen isotope geochemistry of igneous rocks: Contributions to Mineralogy and Petrology, v. 19, p. 1–71, doi: 10.1007/BF00371729.

Taylor, S.R., and McLennan, S.M., 1985, The continental crust: Its composition and evolution: Geoscience Texts: London, Blackwell, 312 p.

Todt, W., Cliff, R.A., Hanser, A., and Hofmann, A.W., 1984, $^{202}Pb+^{205}Pb$ double spike for lead isotopic analyses: Terra Cognita, v. 4, p. 209.

Topuz, G., Altherr, R., Kalt, A., Satır, M., Werner, O., and Schwarz, W.H., 2004, Aluminous granulites from the Pulur complex, NE Turkey: A case of partial melting, efficient melt extraction and crystallization: Lithos, v. 72, p. 183–207, doi: 10.1016/j.lithos.2003.10.002.

Woodhead, J.D., Harmon, R.S., and Fraser, D.G., 1987, O, S, Sr, and Pb isotope variations in volcanic rocks from the Northern Mariana Islands: Implications for crustal recycling in intra-oceanic arcs: Earth and Planetary Science Letters, v. 83, p. 39–52, doi: 10.1016/0012-821X(87)90049-5.

Wörner, G., Moorbath, S., and Harmon, R.S., 1992, Andean Cenozoic centres reflect basement isotopic composition: Geology, v. 20, p. 1103–1106, doi: 10.1130/0091-7613(1992)020<1103:ACVCRB>2.3.CO;2.

Yılmaz, Y., Güner, Y., and Şaroğlu, F., 1998, Geology of the quaternary volcanic centers of the east Anatolia: Journal of Volcanology and Geothermal Research, v. 85, nos. 1–4, p. 173–210, doi: 10.1016/S0377-0273(98)00055-9.

Zartman, R.E., 1974, Lead isotope provinces in the Cordilleran of the western United States and their geological significance: Economic Geology and the Bulletin of the Society of Economic Geologists, v. 69, p. 792–805.

Zindler, A., and Hart, S.R., 1986, Chemical geodynamics: Annual Review of Earth and Planetary Sciences, v. 14, p. 493–571, doi: 10.1146/annurev.ea.14.050186.002425.

Zor, E., Gürbüz, C., Türkelli, N., Sandvol, E., Seber, D., and Barazangi, M., 2003, The crustal structure of the East Anatolian Plateau from receiver functions: Geophysical Research Letters, v. 30, no. 24, doi: 10.1029/2003GL018192.

Manuscript Accepted by the Society 30 December 2005

Geological Society of America Special Papers

Magma-crust interactions and magma plumbing in a postcollisional setting: Geochemical evidence from the Erzurum-Kars volcanic plateau, eastern Turkey

Mehmet Keskin, Julian A. Pearce, Pamela D. Kempton, et al.

Geological Society of America Special Papers 2006;409; 475-505
doi:10.1130/2006.2409(23)